AD-A059 018 WISCONSIN UNIV-MADISON ENGINEERING EXPERIMENT STATION F/G 17/5
INFRARED EMISSION AND SCATTERING FROM THE DENSE PLASMA FOCUS.(U)
JUN 78 G R NEIL, R S POST
AFOSR-77-3196

UNCLASSIFIED AFOSR-TR-78-1171 NL

| OF |
AD
A059018

END
DATE
FILMED
11-78
DDC

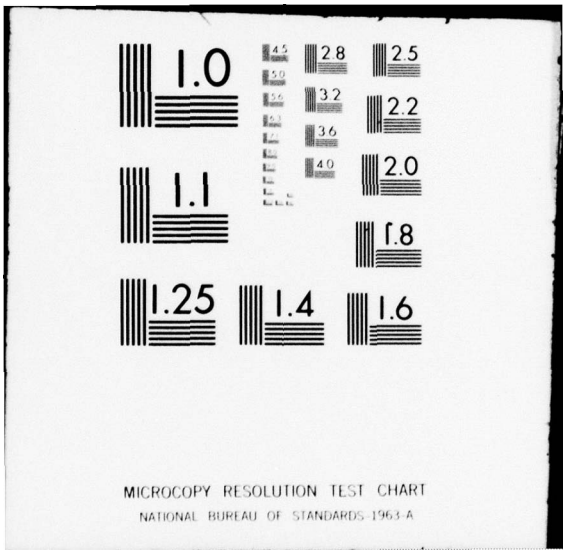
1.0
1.1
1.25
1.4
1.6
2.8
2.5
3.2
2.2
3.6
2.0
4.0
1.8
MICROCOPY RESOLUTION TEST CHART
NATIONAL BUREAU OF STANDARDS-1963-A

LEVEL II

UNCLASSIFIED

SECURITY CLASSIFICATION OF THIS PAGE (When Data Entered)

REPORT DOCUMENTATION PAGE

READ INSTRUCTIONS BEFORE COMPLETING FORM

1. REPORT NUMBER: AFOSR-TR-78-1171

2. GOVT ACCESSION NO.

3. RECIPIENT'S CATALOG NUMBER

4. TITLE (and Subtitle): Infrared Emission and Scattering From the Dense Plasma Focus

5. TYPE OF REPORT & PERIOD COVERED: Final Technical Report covering 1/15/77 - 1/14/78

6. PERFORMING ORG. REPORT NUMBER

7. AUTHOR(s): George R. Neil and Richard S. Post

8. CONTRACT OR GRANT NUMBER(s): AFOSR-77-3196

9. PERFORMING ORGANIZATION NAME AND ADDRESS: Univ. of Wisconsin - Engineering Experiment Station, 1500 Johnson Drive, Madison, WI 53706

10. PROGRAM ELEMENT, PROJECT, TASK AREA & WORK UNIT NUMBERS: 2301 A7, 61102F

11. CONTROLLING OFFICE NAME AND ADDRESS: Director of Physics AFOSR/NP, Bolling Air Force Base, Washington, D.C. 20332

12. REPORT DATE: Jun[redacted]78

13. NUMBER OF PAGES: 64

14. MONITORING AGENCY NAME & ADDRESS (if different from Controlling Office): 65 p.

15. SECURITY CLASS. (of this report): Unclassified

15a. DECLASSIFICATION/DOWNGRADING SCHEDULE

16. DISTRIBUTION STATEMENT (of this Report)

Approved for public release; distribution unlimited.

DDC RECEIVED SEP 25 1978 D

17. DISTRIBUTION STATEMENT (of the abstract entered in Block 20, if different from Report): Final rept. 15 Jan 77-14 Jan 78

18. SUPPLEMENTARY NOTES

19. KEY WORDS (Continue on reverse side if necessary and identify by block number)

Plasma Focus
Infrared Emission
Laser Scattering
High-Voltage

20. ABSTRACT (Continue on reverse side if necessary and identify by block number)

This report describes investigations of the dense plasma focus designed to study turbulent processes. A CO_2 laser collective scattering experiment with a high sensitivity was performed to measure the collective fluctuation spectrum. Scattering was observed from small, overdense regions and was correlated with micropinches seen in soft X-ray photographs. Bremsstrahlung was measured near the electron plasma frequency to determine a possible role for beam plasma instabilities. Only thermal bremsstrahlung levels were detected.

DD FORM 1 JAN 73 1473 EDITION OF 1 NOV 65 IS OBSOLETE

UNCLASSIFIED

SECURITY CLASSIFICATION OF THIS PAGE (When Data Entered)

380 200

AFOSR-TR- 78-1171

LEVEL II

INFRARED EMISSION AND SCATTERING
FROM THE DENSE PLASMA FOCUS

by

June 1978

George Neil and Richard Post

The final report for Grant AFOSR 77-3196 covers the following principal results.

1) The measurement of a thermal bremsstrahlung spectrum near the electron plasma frequency. This suggests electron beam plasma interactions were not a dominant effect in heating of our dense plasma focus.

2) Collective scattering with a sensitivity of $nS_k = 7 \times 10^{19}/cm^3$ failed to detect turbulence near the ion plasma frequency.

3) Scattering revealed micropinches of overdense plasma with transverse scale size of ~40 μm. The pinches correlate with intense X-ray sources observed in high resolution soft X-ray photographs.

Papers Given or in Preparation

1) G. R. Neil and R. S. Post. Infrared Emission and Scattering from the Dense Plasma Focus. Bull. Am. Phys. Soc. 22, 1211 (1977).

2) G. R. Neil and R. S. Post. Multichannel, high-energy railgap switch. Rev. Sci. Instrum. 49, 401 (1978).

3) G. R. Neil and R. S. Post. Overdense Scattering at 10.6 μm in the dense plasma focus. To be submitted to Plasma Physics.

4) G. R. Neil and R. S. Post. Infrared Emission from the Dense Plasma Focus. To be submitted to Plasma Physics.

TABLE OF CONTENTS

LIST OF FIGURES

CHAPTER 1

APPARATUS

The Plasma Focus Device[1] consists of a pair of coaxial electrodes between which an electrical discharge is initiated (See Figure 1). The volume between the electrodes is pressurized to around 2 mm of Hg with hydrogen or deuterium. A sheet discharge forms across the rear insulator and accelerates down the gun due to the $\vec{J} \times \vec{B}$ force, sweeping up and ionizing the gas in the gun. When the current sheet reaches the end of the gun a quasi-cylindrical pinch forms, compressing and heating a portion of the gas that was in front of the center electrode (anode). If the filling pressure is adjusted so that the pinch forms at or just after the current maximum a hot dense filament forms, approximately 15 mm long and 3 mm in diameter, which is called the Dense Plasma Focus (DPF).

This dense phase lasts approximately 40 ns before pinching off in an m = 0 mode. The dense phase is characterized by densities on the order of 10^{19} cm^{-3} and bulk temperatures on the order of 1 keV.[2] The highly non-Maxwellian nature of the focus is indicated by anomalously high X-ray and neutron production.[3] Moreover, after the pinch breaks up, a low density phase forms as the neutron yield increases.[4] Clearly additional heating mechanisms are at work. Specifically, turbulence has been suggested as the heating agent.

The best way turbulence may be observed is to scatter light off of the plasma. Enhanced scattering will occur at a level corresponding to the turbulence in the plasma. Further, in such a case the conservation of energy and momentum require that ω and $\vec{k}$ satisfy the wave conservation laws: $\omega = \omega_1 + \omega_2$, $\vec{k} = \vec{k}_1 + \vec{k}_2$. Frequency resolution of the scattered signal gives the hetrodyned frequency of the wave motion. By choosing a long wavelength laser (10.6 microns) we scatter primarily from those waves whose wavelength is larger than a Debye length, that is, the collective modes of the plasma. In so doing we might expect to see enhanced scattering not only from waves propagating in the plasma but also from any macroscopic eddies. The high levels of X-ray production suggest a tail on the electron velocity distribution function. Since such tails can easily cause enhanced fluctuation levels, there is a strong suggestion that suprathermal scattering should occur. Enhanced scattering has often been seen in experiments such as collisionless shocks. Observation of such scattering from the focus should answer such questions as the level, time history and frequency of the turbulence, and thereby its role in heating the focus. While the focus exhibits several other pathological features in addition to the anomalous neutron and X-ray yields, we studied them only to the extent necessary to determine the relative timing and to monitor proper operation of the focus. Before discussing previous studies in more detail let us look at the experimental apparatus involved: the gun and

the associated diagnostics. A description of the CO_2 laser forms the Appendix.

GUN

Figure 1 shows a cross section of the gun. The rear insulator is designed to initiate the discharge uniformly. Optical access to the DPF is provided through the hollow anode (inner electrode) to compliment viewing ports on the side of the vacuum chamber. Baffles and the glass liner provide protection to the salt infrared transmitting window from the hot plasma by preventing the approach of the discharge. In addition, a large expansion chamber is provided for the plasma in front of the focus.

Substitute electrodes are occasionally used. A solid anode produces a more reliable focus but it limits optical access to viewing through the return current sheet. A second defect is that hot plasma from the focus ablates copper from the anode causing uncertainty in the composition of the plasma and a great increase in soft X-ray line radiation. A group of eight rods arranged cylindrically can be used as a cathode (outer electrode). This "squirrel cage" allows gas to escape from the gun permitting operation at higher pressures, and presumably higher final densities.

The focus is driven by a 135μ F capacitor bank operated at 22 kJ of stored energy. Care was taken to minimize inductance of the bank and its associated switches and transmission line. Parallel plate conductors are used, separated

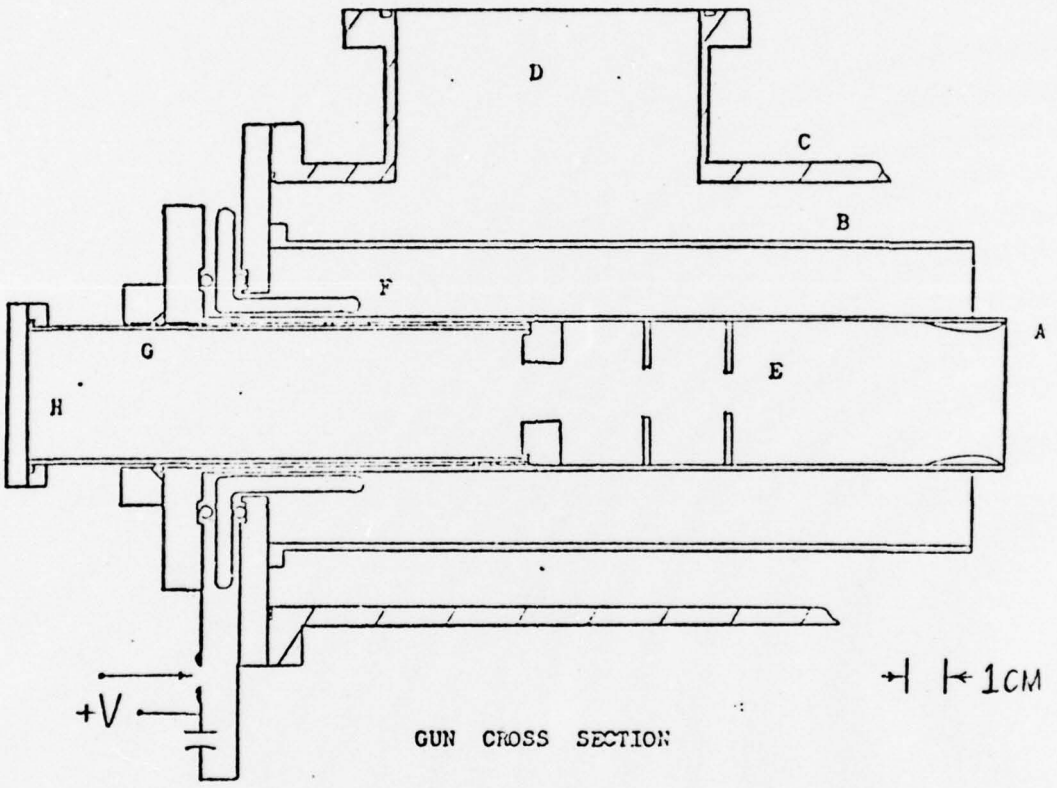

GUN CROSS SECTION

A. Anode
B. Cathode
C. Vacuum Chamber
D. To Vacuum Pumps
E. Baffles
F. Pyrex Insulator
G. Glass Liner
H. Salt Window

FIGURE 1

by 60 mils of polyethylene. The current is switched by a low-jitter railgap. The high currents involved (up to 600 kA peak) imply a high damage rate to the switch unless large surface areas are provided.

Manipulation of the parallel plate conductors allows us to control somewhat the inductance of the system, changing the time of peak current from 3 to 5 microseconds, higher currents being associated with the shorter time.

Current in the focus can be measured using the integrated signal from a current loop located between the parallel plates. The unintegrated signal, proportional to dI/dt, is a more sensitive measure of the time of the focus. The focus occurs just after maximum current when $\frac{dI}{dt} = 0$. Formation of the focus is indicated by a spike in dI/dt caused by the increased inductance of the filament plus any anomalous resistance which may occur. The spike may be used as a timing marker, the absence of which terms the shot a non-focusing event. The amount that the current drops during the focus depends on the inductance of the current source, ranging from 50% to less than 10% (see Figure 2). In either case, the spike is used to compare timing among the various diagnostics which are discussed in the following paragraphs.

DIAGNOSTICS

The DPF is sufficiently energetic to destroy a probe in contact with the plasma. We therefore studied primarily the radiations emitted from the focus while using dI/dt in the

CURRENT AND dI/dt PROFILES

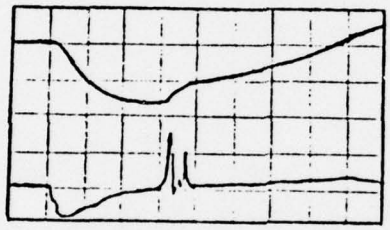

I(200 kA/div)

dI/dt

Low L

C= 90.5 μF

V= 17.8 kV

P(H_2)= 1.6 torr

1 μs/div

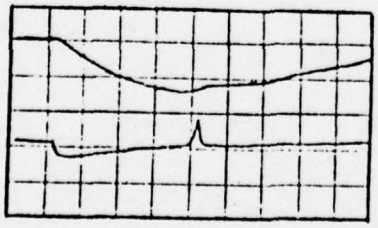

I(240 kA/div)

dI/dt

High L

C= 135 μF

V= 17.8 kV

P(H_2)= 2.4 torr

1 μs/div

FIGURE 2

discharge circuit as a monitor. The following paragraphs briefly describe the detectors used in this study. Schematics of their arrangement will appear later in the section appropriate to each measurement.

INFRARED.

Observation of the infrared emission is important because ω_{pe} radiation from the focus lies in the near infrared region as does the transition from blackbody to volume bremsstrahlung. While it is true that some of the plasma may be inaccessible at frequencies just below ω_p, that is the point where the spectrum should most nearly fit the blackbody formula.[5] Since

$$I_{\omega_{B-B}} = \frac{\omega^2 \, k \, T_e}{4\pi \, c^2} \qquad (\omega << \frac{k \, T_e}{h})$$

dependence on the density is eliminated and a measure of T_e is obtained. Moreover, matching this to the bremsstrahlung formula,[5]

$$I_{\omega_{BREM}} = \frac{16}{3} \frac{n^2 \, e^2}{(4\pi \, \varepsilon_o \, c)^3} \left(\frac{Z \, e^2}{m}\right) \left(\frac{m}{2\pi \, kT}\right)^{1/2} \ln \left(\frac{8k \, T^2}{m \, \omega^2 \, \hbar^2}\right) \cdot V$$

gives a reasonable guess at the density provided one has some idea of the volume and Z. It is fortunate that such effects are in the near infrared region on this device since the visible region is complicated by line radiation

and measurements in the far infrared are more difficult.

The spectral sensitivities are shown in the next figure. It should be noted that the doped germanium detectors can additionally serve to measure scattered laser radiation. Depending on the bandwidth desired, a filter or a grating monochromator is used in conjunction with the detectors. Lead shielding is necessary to prevent X-ray excitation of the detectors. While stacking lead bricks provided marginal shielding, a 4π, cast lead, combination Faraday and X-ray shield was eminently superior.

UV-SOFT X-RAY.

The soft X-ray region is interesting because the energy range corresponds to the temperature of the focus. While no attempt was made to obtain a quantitative measure of the emission in the soft X-ray region, data was taken in several energy bands to facilitate interpretation of the infrared data. A time integrated picture of the focus was taken using a triple pinhole camera with X-ray film. In this manner simultaneous pictures in three energy regions with 25 microns of resolution were obtained. This will be discussed in more detail in Chapter 5. For time dependent measurements silicon PIN detectors with absorption band filters allowed measurements from 400 eV to more than 100 keV.

NEUTRONS

When deuterium is used the neutrons produced give some

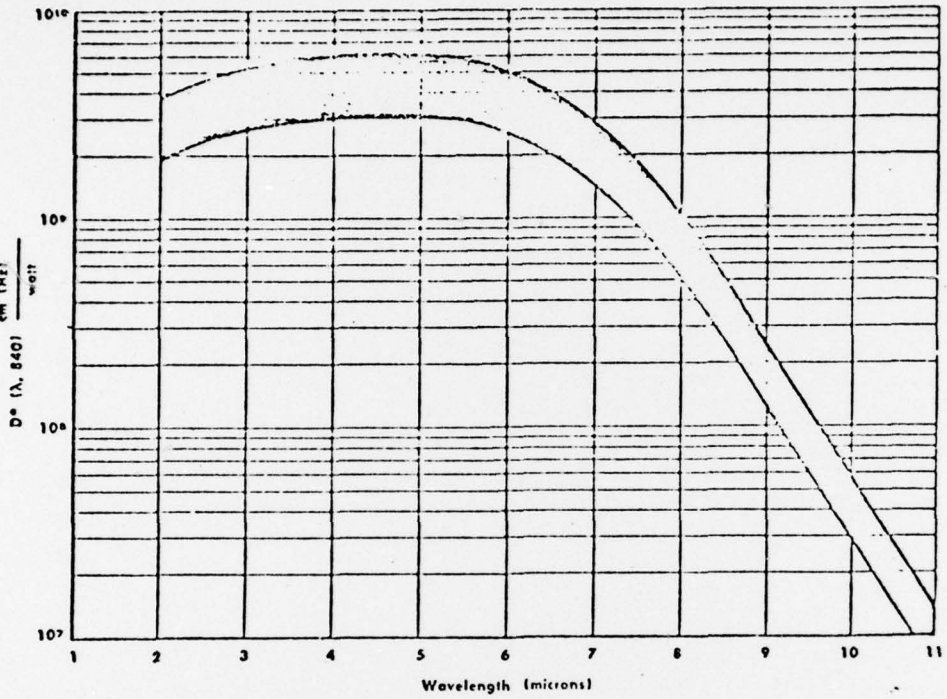

Au Doped Ge Detector (77°K)

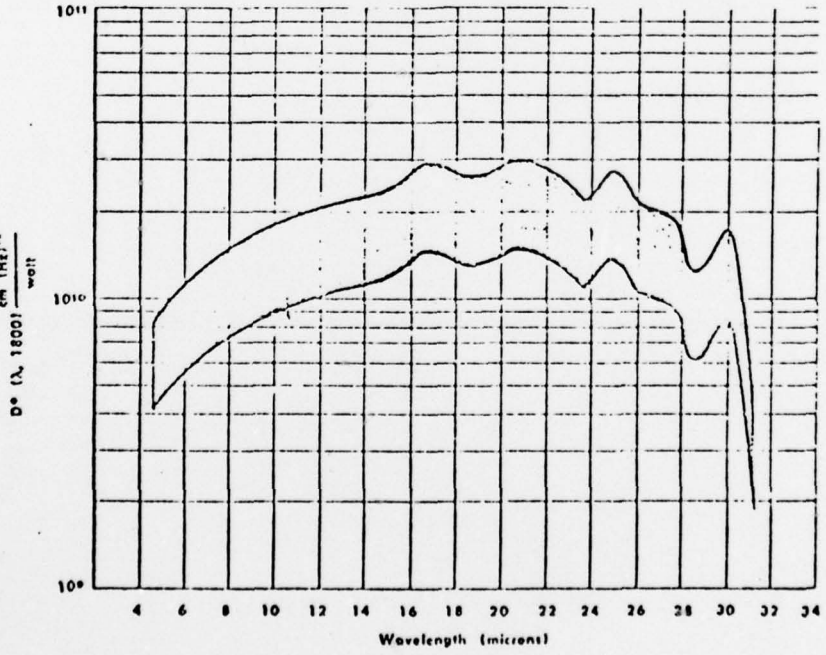

Cu Doped Ge Detector (5°K)

SPECTRAL SENSITIVITIES
FIGURE 3

measure of the effective heating and density although interpretation is not straightforward. A PM tube with scintillating plastic is used for time dependent measurements; it, too, used a 4π cast lead X-ray shield. A time integrated signal is obtained from activating silver foil wrapped around a Geiger tube. A paraffin block thermalizes the neutrons. After the shot the decay of the activated silver is counted on a scaler to obtain a number proportional to the total flux. Calibration is accomplished through use of a standard PuBe source with an appropriate correction for the pulsed nature of the focus. (Pulsed sources activate the silver isotopes by ratio of absorption cross section, whereas the decay rates must be accounted for in steady state cases.)

ASSOCIATED RESPONSE TIMES, ETC.

For all of the time dependent measurements the risetime is of prime importance. Any attempt to unfold the physics of a plasma that lasts 40 ns would be doomed by a detector slower than 20 ns. The infrared detectors and silicon PINs have risetimes on the order of 2 ns while the PM tube limits the neutron detector to about 4 ns. Signal propagation measurements must be made to account for time delays. Fast-rise signals were used to measure cable and scope delay times while an optical pulser measured delay in the PM tube. A time-of-flight correction from the focus to each detector was made. Relative timing errors could in this way be maintained to less than 3 ns.

CHAPTER II

PREVIOUS EXPERIMENTS

This section will summarize parameters found on other devices. We will quote results from devices which operate near the stored energy of our device since we hope to carry over the trend of results, enabling us to predict parameters we cannot measure. We will then conclude this section by estimating plasma parameters in the dense pinch phase on our device. It should be emphasized that we did not attempt to experimentally reproduce all the results of others but only those which were necessary to determine which results carry over to our device.

Although the DPF has been studied for a decade there are as yet many unanswered questions concerning stability and heating mechanisms. Measurements must generally be limited to diagnostics which do not disturb the plasma since anything which disrupts the current sheet will cause the focus not to form. Further, any physical probe would be destroyed by the focus. The most direct thing to do is measure the radiations eminating from the focus.

Measurements of neutron production[3] show a 12% forward to radial anisotropy of the flux (27% front to rear)[1] corresponding to a 500 keV axial source CM velocity. Total neutron production for D-D focuses range from 10^8 to 10^{10}

per shot (or even more with a very large capacitor bank) with a pulse width of up to 200 ns.[1] The duration is significant since the dense pinch lasts about 1/4 that long. Total neuton production is much higher than would be indicated by compressional heating even disregarding the observed anisotropy.[7]

Measurements of the electron and ion temperatures have been made using line ratios of impurity ions[8] and laser scattering[9] which indicate bulk properties of T_e = 2 keV, T_i = .7 keV, and T_{Ar}(4% impurity) - 9 keV. Other measurements on this device[2] (a 42 kJ focus, more energetic than ours) indicate a peak electron density of 4×10^9 cm^{-3} with average values of 8×10^{18} cm^{-3} over a 1 mm radius filament. (There has recently developed some dispute concerning the electron temperature. In contrast to T_e = 2 keV indicated by Peacock[2] above, Bernard[4] claims $T_e < T_i$ with T_e = 100 eV. Luckily the IR emission depends only weakly on the value of T_e; variations in estimates of T_e will cause only minor adjustments in the calculated density.)

The non-Maxwellian nature of the electron velocity distribution is indicated by the soft X-ray production when a solid anode is used. The radiation corresponds to a beam target spectrum with electron energies greater than 100 keV.[3,10] From 5 keV to 350 keV the intensity falls as E^{-2}.[3,11] Activation studies with solid targets in front of the focus indicate ion energies as high as 5 MeV.[12]

An important consideration is the time relationship of

these phenomena. The shot-to-shot variation of the focus is large making concurrent measurements advisable whenever practical. Interferograms[4,13,14] show the high density phase at the time when soft-X-rays begin to appear. Shortly thereafter neutron production begins, peaking at the time of rupture of the focus.[4,14] Recent measurements have shown infrared emission at a level much enhanced above thermal.[15] Collective scattering with a ruby laser showed a highly irreproducible scattered signal at a level corresponding to $S(\vec{k}) \geq 100$ for $|\vec{k}| = 10^4$ cm^{-1}.[4] These occur at times near the breakup of pinch when the neutron yield begins to rise. The laser scattering will be discussed more extensively in Chapter 4.

DISCUSSION

The task of explaining the data with a simple model has not met with success although many models have been proposed. Current theory proposes turbulence as the heating mechanism. Gribkov believes that relativistic electron beams cause this turbulence.[14] Some interferograms show filamentation indicative of the Weibel instability[16] and show self-focusing which could explain the intense X-ray sources seen in pinhole photographs. Alternatively, recent work[17] suggests that radiational collapse can cause these hot spots leaving the ion heating question open. Others have suggested the possibility of ionacoustic instabilities, macroscopic turbulence due to pinching of the plasma column, the electron cyclotron drift instability, and the Buneman instability.[4,14,18] Any or

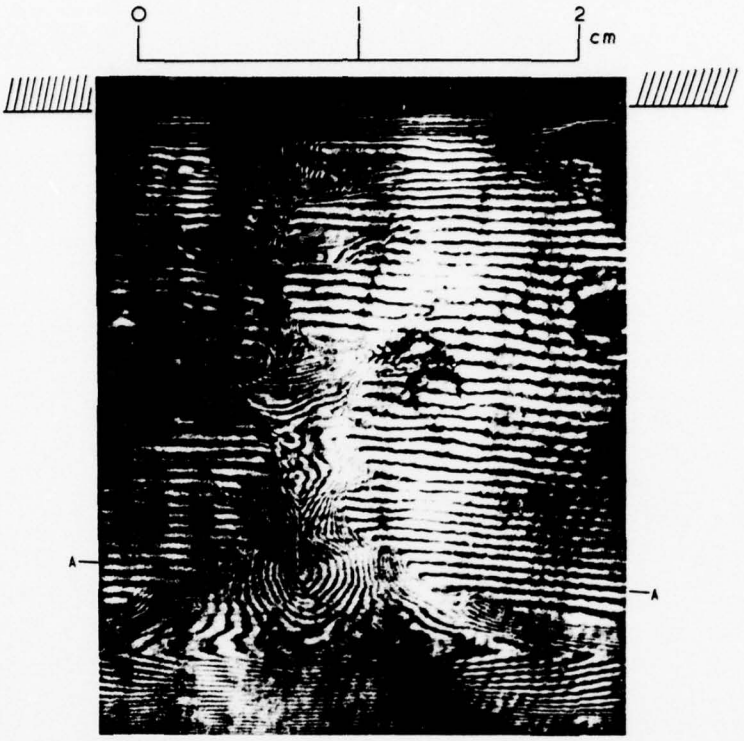

Interferogram of dense pinch at onset of soft X-ray emission (t=0). Exposure time ~ 1 nsec.(2)

FIGURE 4

many of these may be active. It may be that the various instabilities occur in the different parameter ranges which characterize each machine.

Whatever turbulence should happen to exist in the focus the ultimate problem is to connect the turbulence with the heating if indeed they do connect. One possible way would be through anomalous resistivity: energy goes from current carrying electrons to turbulence thence to ions. An alternate route would be to assume that resistance leads to a locally high electric field causing direct acceleration of ions. Sagdeev[19] points out that the ratio of the resistive heating level to classical does not depend on specification of an unstable mode but only on comparison of the wave phase velocity with some mean drift velocity of the electrons. Therefore in either case discussed above, the exact determination of a mode type is unnecessary if one has an idea of the spectrum of such turbulence. This may also explain how several devices can show dissimilar features yet scale in neutron production.

The fact that the DPF is not widely regarded as a fusion power candidate may be attributed to uncertainty about the heating mechanism(s) and its subsequent scaling, in addition to the problems of dealing with insulator tracking at high voltages. On an empirical basis the prospects for a breakeven plasma focus appear bright as may be seen in the next figure.

To conclude we will estimate our plasma parameters

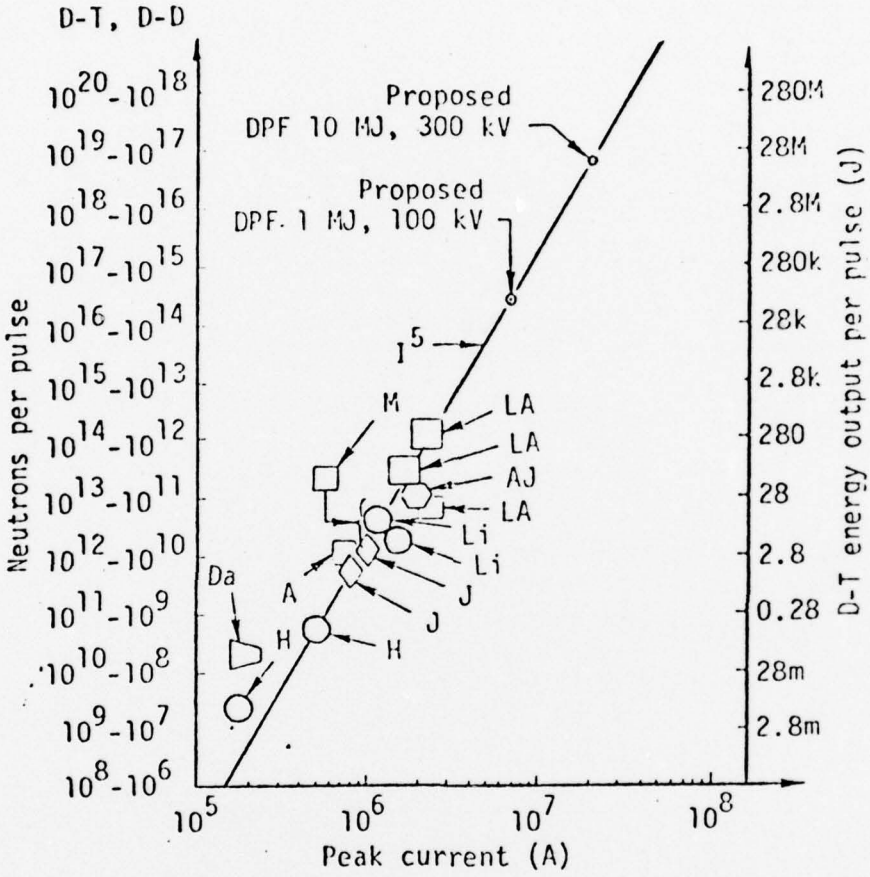

LEGEND

AJ Aerojet Nucleonics
Da Darmstadt.
H Hoboken
A Aerospace Corporation
J Julich
Li Limeil
La Los Alamos
M Moscow

(20)

FIGURE 5

during the dense pinch phase. We have assumed that the density is proportional to filling pressure, $\beta = .6$, and took $T_i = T_e/3$ as indicated by earlier results.[2] By taking the radius of the focus as 1.5 mm, a pressure balance gives T_e (See Table 1). With these estimates in mind we present in Chapter 3 the infrared measurements taken to give an accurate measure of the density.

Table 1

Focus Parameter Estimates - Dense Pinch Phase

n	4×10^{18}	cm^{-3}
T_i	400	ev
T_e	1.2	keV
T_{Ar}	5.7	keV
t_{DEFL}	6×10^{-11}	sec
t_{DD}	3×10^{-9}	sec
$t_{e\text{-}i\ equil}$	1.3×10^{-6}	sec
$\ln \Lambda$	12.7	
λ_D	.13	microns
ω_{ce}	1×10^{13}	sec^{-1}
ω_p peak	1×10^{14}	sec^{-1}
#e/Debye sphere	3.5×10^4	

Known Parameter Operating Limits

E bank	12-22 kJ
$\tau/4$	$3\text{-}5 \times 10^{-6}$ sec
I peak	300-500 kA
Fill Pressure	.5-2.5 torr
Neutrons/shot	$\leq 2 \times 10^9$

CHAPTER 3

INFRARED EMISSION FROM THE FOCUS

In this chapter we will give the results of two experiments measuring the infrared emission from the focus. The rationale behind these experiments is twofold: a determination of n^2Z^2 and T_e can be made, and possibly nonthermal emission can be observed.

The optical configuration is shown in the next figure. It allows measurement at 90° or 180°. While the 180° system does not view the focus through the return current sheet as at 90°, longitudinally local emission might be masked by a volume averaging effect. The experiment is relatively easy to perform. Interpretation is not, however, straightforward. The following caveats must be issued:

a. The shot-to-shot variation of the DPF is large. Structure may vary to some extent and magnitude of the IR signal varies by as much as a factor of two. The curves we present are averages of "typical" measurements, i.e. we have eliminated obvious non-focusing shots and, more subjectively, an occasional pathological shot.

b. Even if the focus were quite reproducible a determination of absolute intensities would still be difficult. Absorption by the atmosphere is

I R EMISSION MEASUREMENT

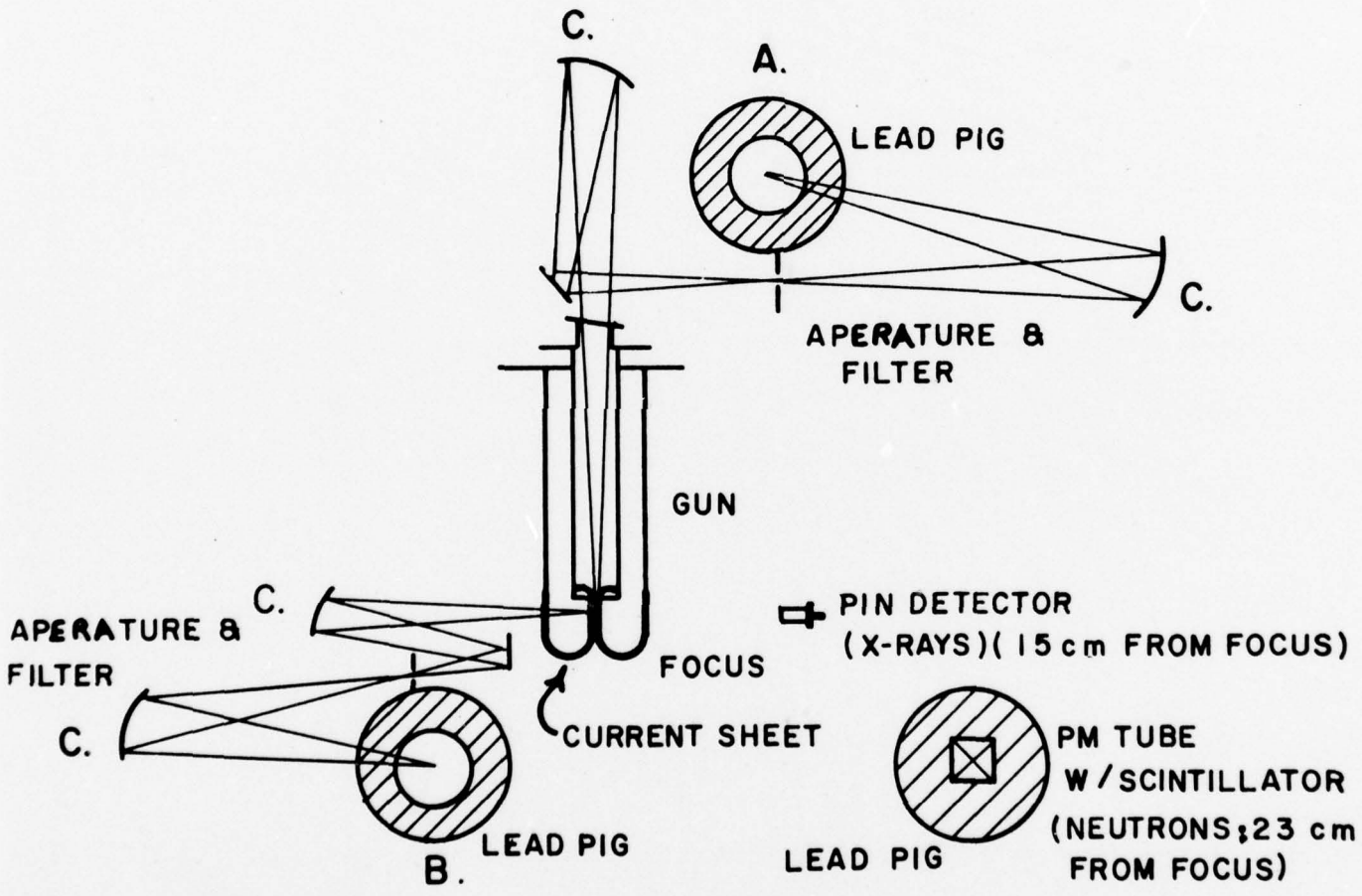

A. Cu-Ge DETECTOR IN 180° EMISSION ARRANGEMENT

B. Cu-Ge DETECTOR IN 90° EMISSION ARRANGEMENT
(VIEWS THROUGH ABSORBING CURRENT SHEET)

C. CONCAVE MIRROR 30cm F.L., 4" DIA.

FIGURE 6

variable dependant on temperature and humidity. Salt vacuum windows are etched by the plasma and metal vapor is deposited. Attempts to compare measured filter transmission with curves provided by the vendors tended to vary by about $\pm$ 30%. In the following analysis we will use the vendors data except in the case of the salt windows whose transmission we measured and the throughput of the grating monochrometer which was also measured. The resulting uncertainties are thought to be much smaller than the shot-to-shot variation.

c. Finally, for a given wavelength some of the plasma may be inaccessible: $\omega < \omega_p$. For all but the most gradual profiles this would mean I would fall off faster than λ^4 as predicted by the blackbody formula. We will discuss the conditions under which this occurs more fully below, but with the above disclaimers in mind we will now present our results.

The next two curves show the measurement of the IR spectrum at 180° and 90°. At 180° there is no signal at -50 ns. Both curves display clearly the transition from thick to thin body emission. Since emission and absorption are peaked near ω_p due to the inverse dependence on the index of refraction, there is a natural tendency for the transition

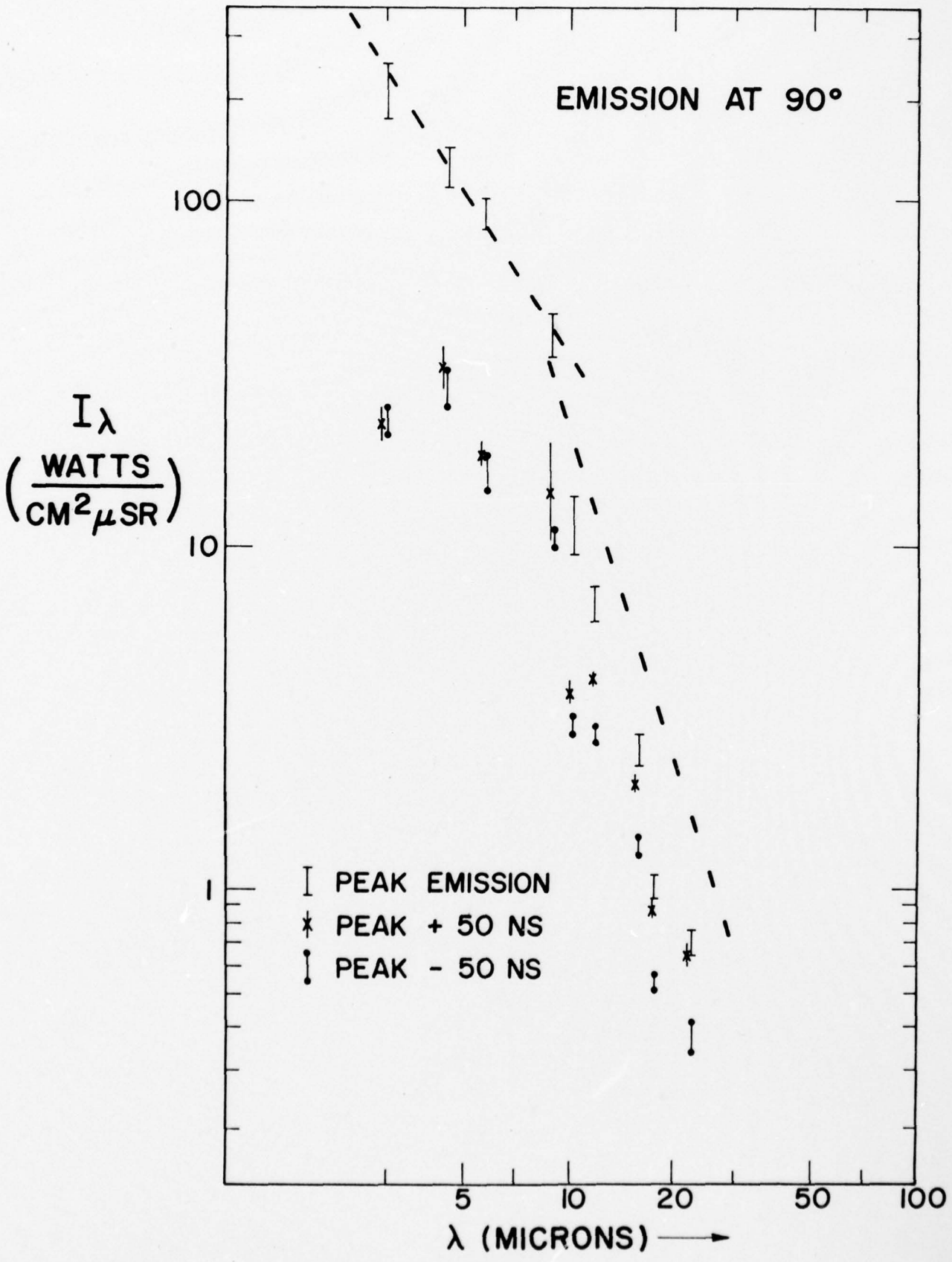
EMISSION AT 90°
100
10
1
I_λ
$\left(\frac{\text{WATTS}}{\text{CM}^2\mu\text{SR}}\right)$
PEAK EMISSION
PEAK + 50 NS
PEAK - 50 NS
5
10
20
50
100
λ (MICRONS) ⟶

FIGURE 7

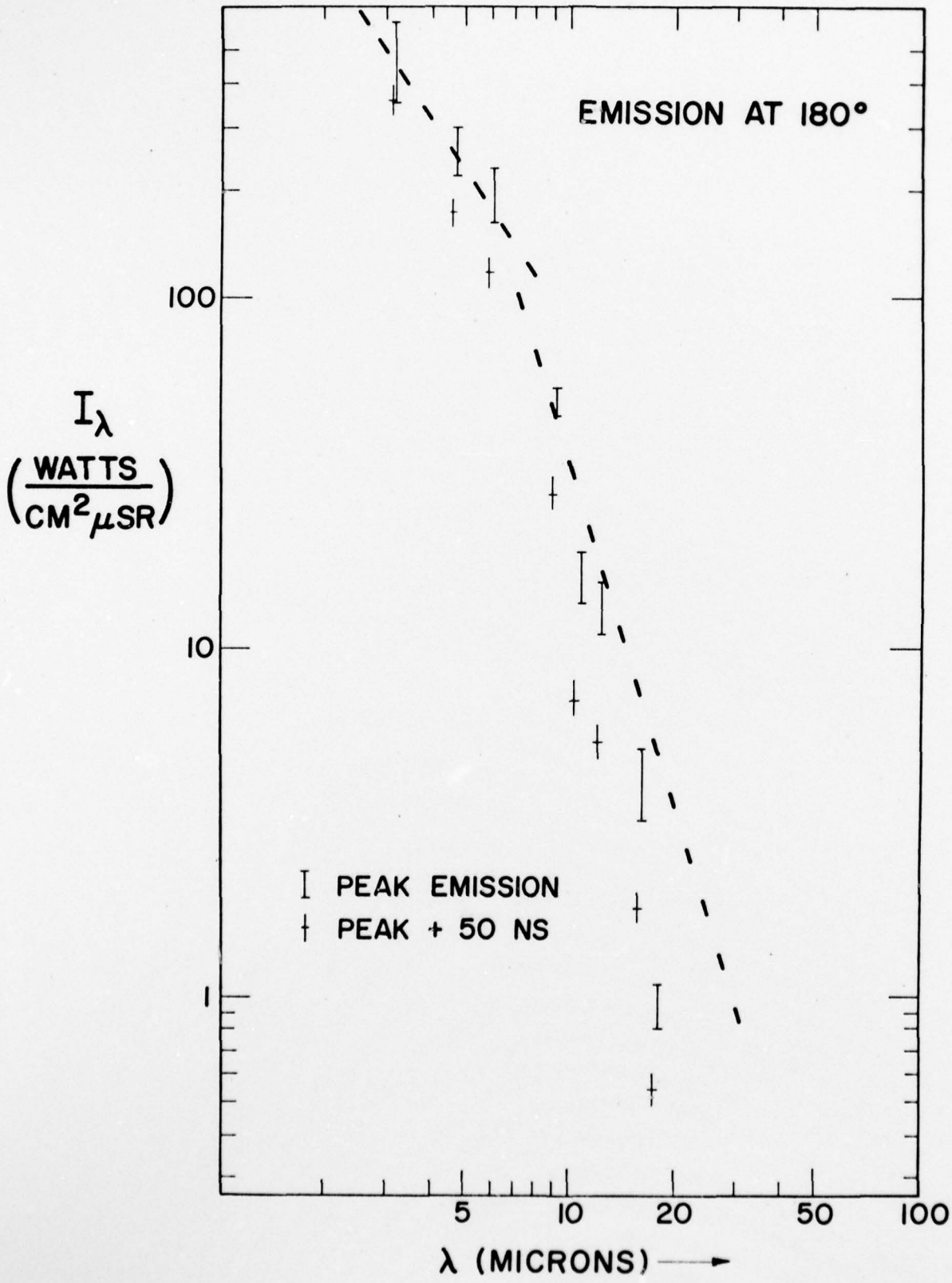
EMISSION AT 180°
100
10
1
I_λ
$\left(\frac{\text{WATTS}}{\text{CM}^2\,\mu\text{SR}}\right)$
PEAK EMISSION
PEAK + 50 NS
5
10
20
50
100
λ (MICRONS) ⟶

FIGURE 8

to take place near ω_p. For frequencies less than ω_p some of the plasma is inaccessible. Ideally, if one considers emission at a frequency just above ω_p (peak) then that emission should most nearly approach both bremsstrahlung and blackbody radiation. This point is evident as the break in the $1/\lambda^2$ curve.

$$I_{\lambda_{B\text{-}B}} = T_e \, c/\lambda^4$$

Thus $$T_e = I_\lambda \frac{\lambda^4}{c}$$

For $$\lambda = 10\mu, I_\lambda = 20 \frac{W}{cm^2 \, \mu \, SR}$$

$$T_e = 41 \text{ eV}.$$

Since we know that the focus has an electron temperature on the order of 1 keV we must discard the idea that what we see is blackbody emission. One might think that any time a critical surface is approached, blackbody emission at that frequency will result because of the zero in the dielectric function. This is not true; we can derive the conditions under which this occurs. (In the following section only, n refers to refractive index and N to density).

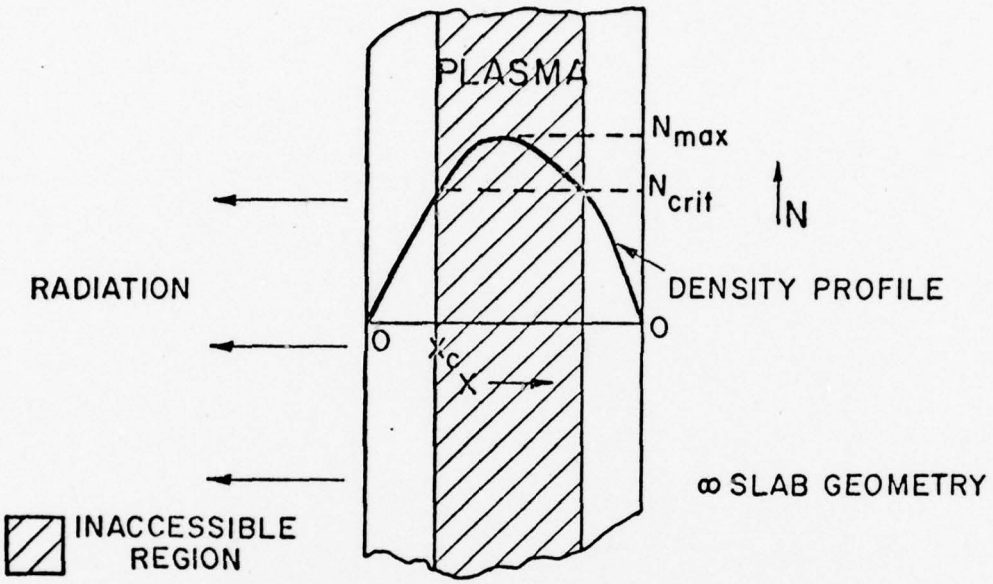

CONDITIONS FOR BLACKBODY EMISSION

We postulate a density profile such that $N(x) = N_{crit} f(x)$, $f(0) = 0$. That is, some given ω is the plasma frequency for N_{crit}. Note that N_{max} is not necessarily equal to N_{crit}. That portion of the plasma that lies within a region such that $N > N_{crit}$ will internally have a blackbody limited intensity. To escape, this radiation must pass through the region where the refractive index (n) changes rapidly causing reflection. The next figure shows how rapid this change can be depending on collisionality. Both the rapid change and its dependence on ν is obvious upon perusal of the formula for n given below. If the change in n occurs over a distance short compared to the wavelength considered the

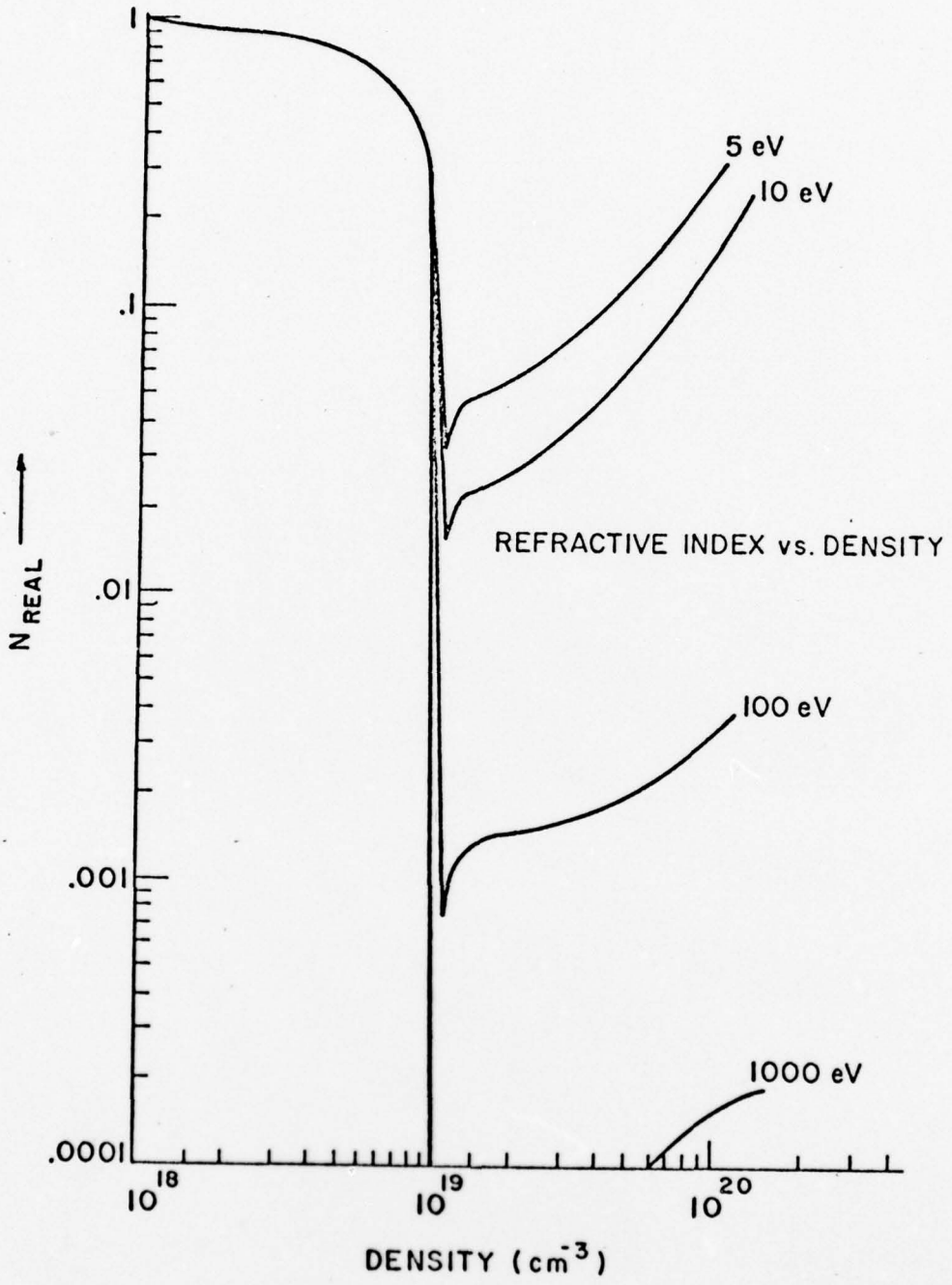
1
.1
.01
.001
.0001
N REAL
5 eV
10 eV
REFRACTIVE INDEX vs. DENSITY
100 eV
1000 eV
10^{18}
10^{19}
10^{20}
DENSITY (cm^{-3})

FIGURE 9

transmission is

$$T = \left(\frac{2\, n_1/n_2}{1 + n_1/n_2}\right)^2$$

The scale length for a change in n is calculated as follows:

$$n^2 = 1 - \frac{\omega_p^2}{\omega^2} \frac{1}{1 + i\,\nu/\omega} \qquad [21]$$

Thus $n_{REAL} = \sqrt{1/2\ (A + B)}$

where $A^2 = B^2 + \left[\frac{\nu}{\omega}\left(\frac{\omega_p^2}{\omega^2 + \nu^2}\right)\right]^2$, $B = 1 - \frac{\omega_p^2}{\omega^2 + \nu^2}$.

Then the gradient is $\left.\frac{\partial n_R}{\partial N} = 1/4 \frac{\frac{\partial A}{\partial N} + \frac{\partial B}{\partial N}}{n_R}\right)_{\omega = \sqrt{\omega_p^2 - \nu^2}}$

$$= 1/4 \frac{e}{m\, \varepsilon_o\, \nu\, \omega_p} .$$

This yields $\left.\frac{\partial n_R}{\partial x}\right)_{x = x_c} = 1/4 \frac{\omega_p}{\nu} \frac{1}{N} \frac{dN}{dx}_{x = x_c}$.

For T_e = 1 keV and $n_e = 10^{19}$ cm^{-3}, $\frac{\omega_p}{\nu} = 3.2 \times 10^4$. This means one scale length for a change in refractive index is less than a micron for a density scale length less than 80 meters, a condition which is always met. For these same parameters at 11 microns n_r is less than 10^{-4} and T is less than 4×10^{-8}. Little of the radiation escapes from inside N_{crit} so we turn our attention to the total radiation emitted from x = 0 to x = x_{crit}

For small ν/ω, $\alpha = (\nu/c) \dfrac{\omega_p^2}{(\omega^2 + \nu^2)\sqrt{1 - \omega_p^2/\omega^2}}$

$$\left.\frac{dI}{dx}\right|_{ABS} = -\alpha_\omega I$$

if $$Q \equiv \int_o^{x_c} \alpha_\omega(x)\, dx >> 1$$

total absorption and consequently blackbody emission results. Ignoring the log dependence of ν we take

$$\nu_o = \nu_o\, f(x)$$

$$N = N_c\, f(x) \qquad (f(x_c) = 1.)$$

$$Q = \frac{\nu_o}{c} \int_o^{x_c} \frac{f^2(x)\, dx}{\sqrt{1 - f(x)}}$$

Whether we have blackbody emission is determined by an absorption length times a geometrical factor of order one dependent only on the density profile.

$f(x)$	$\int dx = Q\, c/\nu$
x	$1.07\, x_c$
x^2	$.59\, x_c$
$\sqrt{x}$	$1.37\, x_c$
$4\sqrt{x}$	$3.0\, x_c$

Thus to zeroth order we may use $\dfrac{\nu\, x_c}{c}$ as our blackbody criterion. For $N = 10^{19}$ cm^{-3}, $T_e = 1000$ eV, $\nu_o\, x_c/c$ is about .02 for the focus, i.e. much less than 1. We will therefore not see blackbody emission.

PEAK AND RMS DENSITY

What we do see is the bremsstrahlung emitted from a smaller and smaller portion of the plasma. Attempts to unfold the rate of fall-off into a density profile were unsuccessful due to the complicated dependence on both the product N^2V and reflection from the critical surface. We can obtain, however, both peak and RMS density. The peak is given as the critical density for the wavelength at the departure from $1/\lambda^2$ dependence. The observed break at 5.5 microns gives an N of 3.7×10^{19} cm^{-3}. Solving the bremsstrahlung formula for N^2:

$$N^2 = 6.02 \times 10^{33} \frac{I_\lambda \lambda^2 T_e^{1/2}}{g Z L}$$

$I(W/cm^2 \mu sr)$, λ (microns), $T_e(eV)$, L(cm). For $Z = 1.6$, $g = 2$, $L = .3$ cm, $T_e = 1200$ eV, $\lambda = 5\mu$, then $n = 2.3 \times 10^{19}$ cm^{-3}.

This is reasonable considering Peacock's published peak to average density ration of 4.[2]

The emission before and after the peak compression is not so easily understood. The break has now moved to 11 microns which would correspond to a critical density of 9×10^{18} cm^{-3}. This is much larger than the 1×10^{17} cm^{-3} indicated by interferograms.[2,4] An alternative explanation would be absorption/emission by a 10 eV plasma. For a 10 eV plasma at 10^{18} cm^{-3} one absorption length is .5 cm which is about the current sheet thickness indicated by the inter-

ferograms of Bernard, et al.[4] Thus we envision the emission spectrum as resultant of two effects; imagine a plasma with an inaccessible region as shown above, viewed through another absorbing plasma (the return current sheet).

CURRENT SHEET EFFECTS

It is important to note that although emission and absorption are related processes the optics are focused on the dense pinch and thus discriminate against emission by the current sheet. This emission is characterized by its lack of time dependence and low blackbody temperature and only became significant at the longest wavelengths.

An independent measurement of the current sheet absorption was obtained by a 10.6 micron transmission experiment. At this wavelength a relatively constant value of 70% sheet was obtained, in agreement with the emission data. The 180° emission data is ambiguous in that we cannot discount the possibility of either a high density area or a cool absorbing plasma at +50 ns. Resolution of this question would require a simultaneous laser interferogram. Published interferograms show both a high density area and a larger, presumably cooler, nose in front of the afterglow.[4] We assume a similar stucture behind the focus in our hollow electrode case. This uncertainty limits the accuracy of our laser scattering data. We may assume the worst case, i.e. when all of the falloff at 10 microns is due to absorption by cool plasma and take

this is to calculate a lower limit to the incident laser intensity. An axial 10.6 micron transmission measurement showed refraction but little absorption during the pinch and large absorption after the pinch broke up.

NONTHERMAL EMISSION

Contrary to expectation, nonthermal emission[7,15] was not observed during the emission spectrum measurement. Nonthermal emission is emission above the thermal level and is generally associated with three wave processes. The observation of such emission would be indicative of strong density fluctuations as might occur at the plasma frequency. To place a limit on the magnitude of any nonthermal emission we used the spectograph with a beam splitter to observe harmonically related bands simultaneously. A .1 micron bandwidth was used at 10 microns (.05 at 5 microns). Out of 80 shots only 4 shots yielded an intensity variation differing by 2 or more. In each anomalous case the 10 micron signal was enhanced above the 5 micron with a maximum enhancement of about 6. This is in stark contrast to the earlier results of Post[7,15] who observed enhancement in 50% of his shots with the power increasing by an order of magnitude or more. We have no explanation of this but note that the only major difference between our machines are the operating voltages and the source impedence.

The preceeding paragraphs have given not only the density of the focus but also the current sheet absorption. These values determine the calibration and sensitivity of the laser scattering experiment discussed next. The theory of collective scattering is treated first, followed by the experimental results and a discussion of their implications.

CHAPTER IV
LASER SCATTERING

This chapter gives the results of the laser scattering experiment. To form a foundation on which to discuss the implications of such results, the first section discusses the theory of laser scattering with an emphasis on collective scattering. This is followed by a summary of two similar experiments by other researchers showing the advantage of our technique. Although our experiment was originally justified as a collective laser scattering experiment, the results indicated scattering from previously unexpected small overdense regions occuring after breakup of the pinch. The final section of this chapter outlines the evidence leading to this decision including the temporal relationship between the scattered signal and the other diagnostics.

THEORY

When light is scattered from a plasma the product is not just the incident intensity times the individual electrons' Thompson cross sections. The scattering is a cooperative venture involving not only the basic plasma properties but also the fluctuation level of the plasma. That is, scattering involves the incident wave and a wave in the plasma. Such ideal three wave processes are collisions in

the classical sense in that momentum and energy are conserved. Thus for the scattered wave:

$$\vec{k}_{SCATT} = \vec{k}_{INC} + \vec{k}_{PLASMA}$$

$$\omega_{SCATT} = \omega_{INC} + \omega_{PLASMA}$$

The character of the scattered spectrum depends on the parameter $\alpha = \frac{1}{k\lambda_D}$ ($k = |k_{PLASMA}|$, λ_D is the Debye length = $740 \frac{T_e(eV)}{n_e(cm^{-3})}$ cm). If $\alpha << 1$ collective effects cannot appear and the scattering is termed incoherent. This is the conventional scattering experiment wherein one observes broadening due to the electron temperature. If $\alpha >> 1$ only long wavelengths contribute to give cooperative scattering. In cooperative scattering the electrons seen are those coupled to the ions' motion or some other long wavelength phenomina. This is the reason for performing a collective laser scattering experiment on the focus. Although there is good evidence that the dense pinch exhibits near thermal levels of scattering (as we discuss below), the post pinch plasma is not expected to be thermal if turbulence is contributing to the ion heating. Turbulence enhances the scattered power; enhancements of 10^4 have been observed in collisionless shocks.[23] In a collisionless Z pinch enhanced scattering was observed with a broadened central line indicating plasma turbulence with a $\Delta\omega \leq \omega_{pi}$.[29] Such turbulence is invoked to explain the structure and collisionless heating in shocks.

The form factor which describes the scattered power is $S(\vec{k},\omega)$. The scattered power is given by

$$P(\vec{k},\omega)\, d\omega\, d\Omega = N_e\, I\, \sigma\, S(\vec{k},\omega)\, d\omega\, d\Omega$$

where N_e is the number of scattering electrons, I is the incident intensity, σ is the Thompson cross section, $d\omega$ is the frequency interval, and $d\Omega$ the solid angle of collection. $S(\vec{k},\omega)$ is the spectral density function of fluctuations in the plasma density. For a collisionless, low temperature, thermal plasma $S(\vec{k},\omega)$ may be explicitly calculated in terms of the electron and ion parts of the dielectric function $\varepsilon = 1 + G_e + G_i$. This is a complicated function even for the relatively simple case of a Maxwellian distribution (see Sheffield[22] eq. 6.3.11).

To determine the fluctuation level in the plasma we need to determine the value of S_k. That is, for a given value of $\vec{k}$ what is the scattered signal integrated over frequency. Using the integral of the Salpeter function[22] (Maxwellian, unmagnetized plasma, $T_e = T_i$):

$$S_k = \frac{1}{1 + \alpha^2} + \frac{1}{1 + \alpha^2} \frac{Z\, \alpha^4}{1 + \alpha^2 + \alpha^2\, Z(T_e/T_i)}$$

The first term is the electron feature (electron plasma frequency satellites); the second is the ion feature (central line). For small α in a thermal plasma the electron feature dominates and vice versa. In a plasma with superthermal levels of turbulence collective scattering would be enhanced

at the sum of the laser frequency and the frequency of the wave turbulence. From the infrared emission the focus has a $\lambda_D = .1\ \mu$ during the dense pinch and $\lambda_D = .7\ \mu$ post pinch. For a 90^o scattering using a CO_2 laser the value of α should range from 12 during the pinch to 1.7 post pinch. For any value of $\alpha \sim 1$, $S_T \approx 1/2$ for a thermal plasma; enhanced turbulence would increase that greatly.

PREVIOUS WORK

On the DPF two major collective scattering experiments have been performed.[4,9] Table 2 summarizes those experiments. In each case thermal scattering was observed during most of the pinch with an enhancement of short duration near the end of the period. Note that both experiments used a ruby laser. This makes possible higher sensitivity and better frequency resolution than with CO_2 but has a weakness in that α is down by 15.4 for a given scattering angle. With a CO_2 laser we are able to remain collective longer (to lower densities and higher electron temperatures). In stressing this advantage it is important to be wary of refraction of the laser beam in the CO_2 case; the critical density is 10^{19} cm^{-3} versus 2×10^{21} with ruby light. Since the plasma achieves the critical density for CO_2 during the dense pinch light may be refracted into the collection mirrors. Such a problem should not exist post pinch. Refraction may be identified by arranging the incident electric vector collinear with the detection optics so that no scattering should be observed,

Table 2

Summary of Collective Scattering

Gun & Pinch Parameters

	Bernard, et al.[4]	Forrest, et al.[9]
Bank Energy	27 kJ	42 kJ
Filling Pressure	3 torr D_2, 5% Ar	2.5 torr D_2, 4% Ne
Peak Current	.5 MA	1. MA
n_e peak	5×10^{19} cm^{-3}	2×10^{19} cm^{-3}
T_e	~ .2 keV	2.2 keV
T_i	.7 keV	.7 keV
α	12	1.8
Level of Scattering	thermal	thermal

Late & Post Pinch Results

Maximum S_k	$\geq$ 100	~3
Time of occurence	t = +50 ns (t = 0 start of neutron emission)	t = 50 ns → when pinch breaks up (t = 0 maximum compression)
Duration	< 10 ns	< 10 ns
Frequency shift corresponds to bulk velocity of	1.8×10^7 cm/sec	2-3 $\times 10^7$ cm/sec
Line shape	single or double humped	double humped

Laser Parameters

Type	Ruby	Ruby
Scattering Angle	7°	45°

only the refracted signal (this will be clearer when the optical set-up is diagramed in the next section).

EXPERIMENT

Since previous attempts by others to see scattered CO_2 radiation had been unsuccessful,[9,24] a highly sensitive [$D^*(10.6) = 1.5 \times 10^{10}$ cm$\sqrt{\text{Hz}}$/W] cryogenic Cu:Ge detector was used.[6] Operating with a preamplifier the sensitivity was 37.5 V/W with a bandwidth of 100 MHz and a noise level of 10 mV. Without preamplification, the corresponding values are .75V/W, 400 MHz, and 2 mV, respectively. The detectors were used in the optical arrangement indicated in the next figure.

To limit the amount of bremsstrahlung observed and to obtain frequency resolution of the scattered signal, a 30 cm F.L. monochromator was used. Using a 100 line/mm grating the resolution limit was .02 microns, measured with the CO_2 laser light.

Several factors limited the sensitivity. As mentioned in the previous chapter, absorption of the incident and scattered beam was measured as 70%/sheet. With a 10 μ bandpass filter the monochromator had a measured transmission of 25%. The 20 MW peak power laser (See Appendix) was focused to a 3 mm spot size to guarantee coincidence of the beam and the dense pinch. This limited the incident intensity and therefore the detection ability. This also limited the intensity to a value below the experimentally observed threshold for

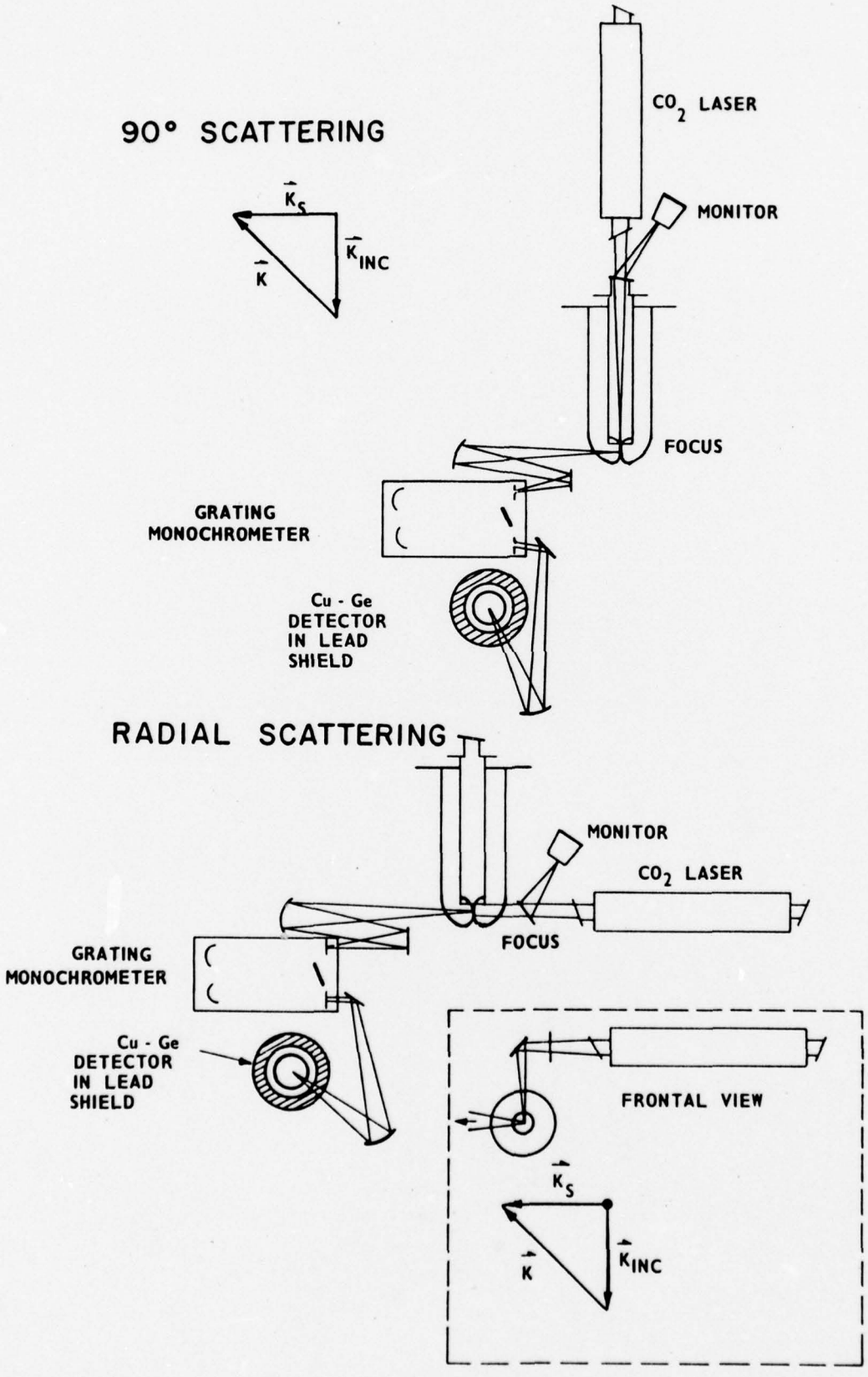
90° SCATTERING
$\vec{K}_S$
$\vec{K}_{INC}$
$\vec{K}$
CO_2 LASER
MONITOR
FOCUS
GRATING
MONOCHROMETER
Cu - Ge
DETECTOR
IN LEAD
SHIELD
RADIAL SCATTERING
MONITOR
CO_2 LASER
FOCUS
GRATING
MONOCHROMETER
Cu - Ge
DETECTOR
IN LEAD
SHIELD
FRONTAL VIEW
$\vec{K}_S$
$\vec{K}$
$\vec{K}_{INC}$

FIGURE 10

induced Langmuir turbulence.[9]

For a 1:1 signal to noise ratio, the minimum visible nS_k is given by $nS_k = \Delta P/(I\ \sigma\ V\ \Delta\Omega) = 7 \times 10^{18}$ cm^{-3} (ΔP - the minimum observable power at 1:1 signal to noise ratio divided by the total transmission loss = 13 mW; I - the incident intensity = 2.8×10^{8} W/cm^2; σ - the Thompson cross section = 8×10^{-26} cm^2; V - the scattering volume = 10^{-2} cm^3; $\Delta\Omega$ - the collection solid angle = 7×10^{-3} sr). Interferometric data on similar experiments[4] indicate that the density during the dense pinch is about 5×10^{18} cm^{-3} over the scattering volume. Thus a value of $S_k \gtrsim 1$ should be visible.

When the measurement was made, similar scattering levels ($nS_k = 7 \times 10^{19}$ cm^{-3}) at two different scattering angles (as indicated in Figure 10) suggested a scattering experiment with unfavorable polarization -- collection optics collinear with the incident wave electric vector in the scattering volume (See Figure 11 -- the scattering electron oscillates toward and away from the collection optics and therefore radiates no transverse oscillating $\vec{E}$ field in the direction of the collecting mirror). Instead of null result expected, scattering of the same level occured. This can be explained as refraction or reflection from a critical surface. Although the resolution of the monochromator was sufficient to resolve sidebands shifted by an $\omega \geq 4 \times 10^{11}$ sec^{-1} corresponding to an ω_{pi} for a density of 10^{17} cm^{-3} and was sufficient to detect a Doppler shift ($\Delta\lambda = 2\ v/c\ \lambda_o \sin \theta/2$)

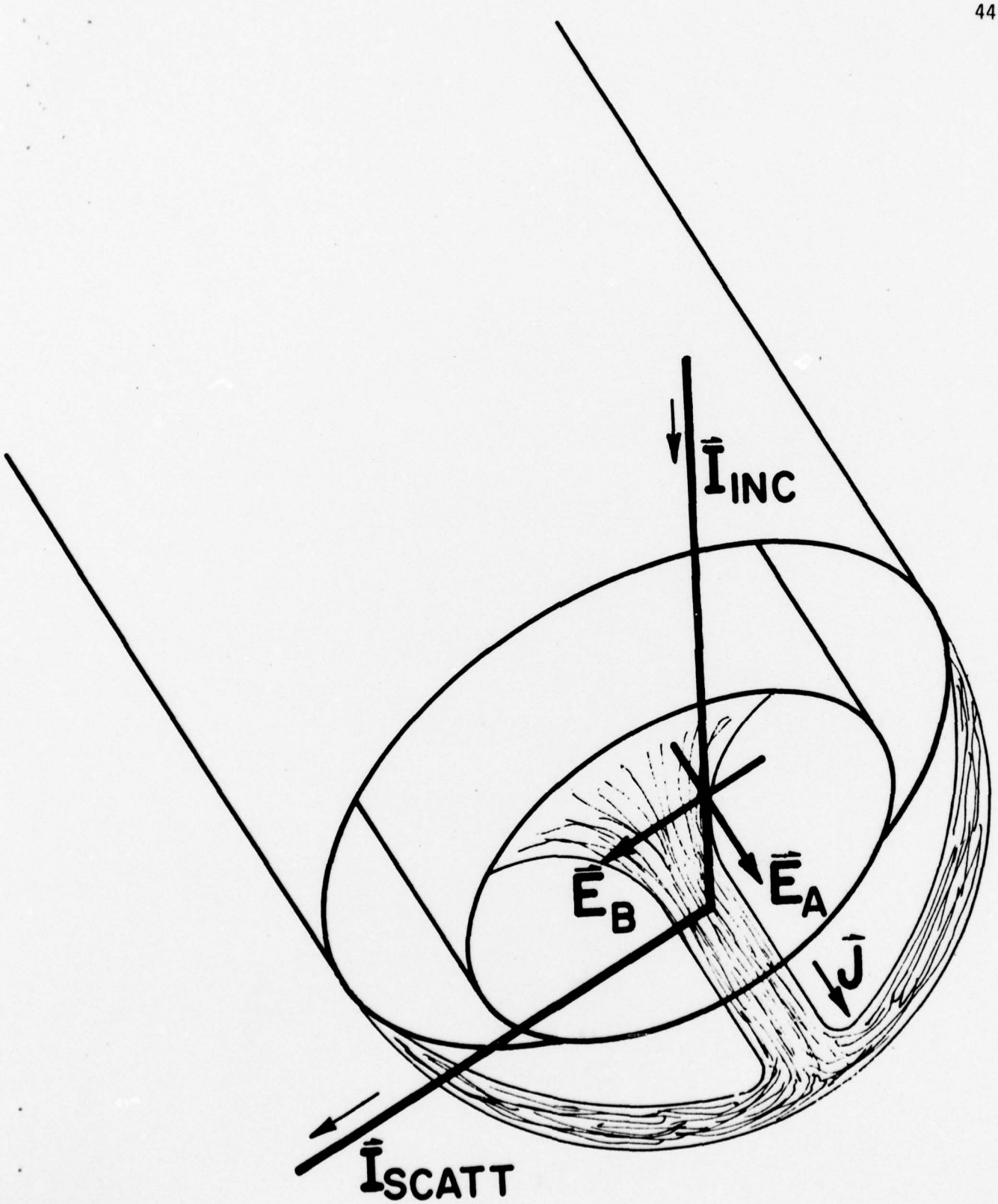

SCATTERING POLARIZATION : E_A favorable E_B unfavorable

FIGURE 11

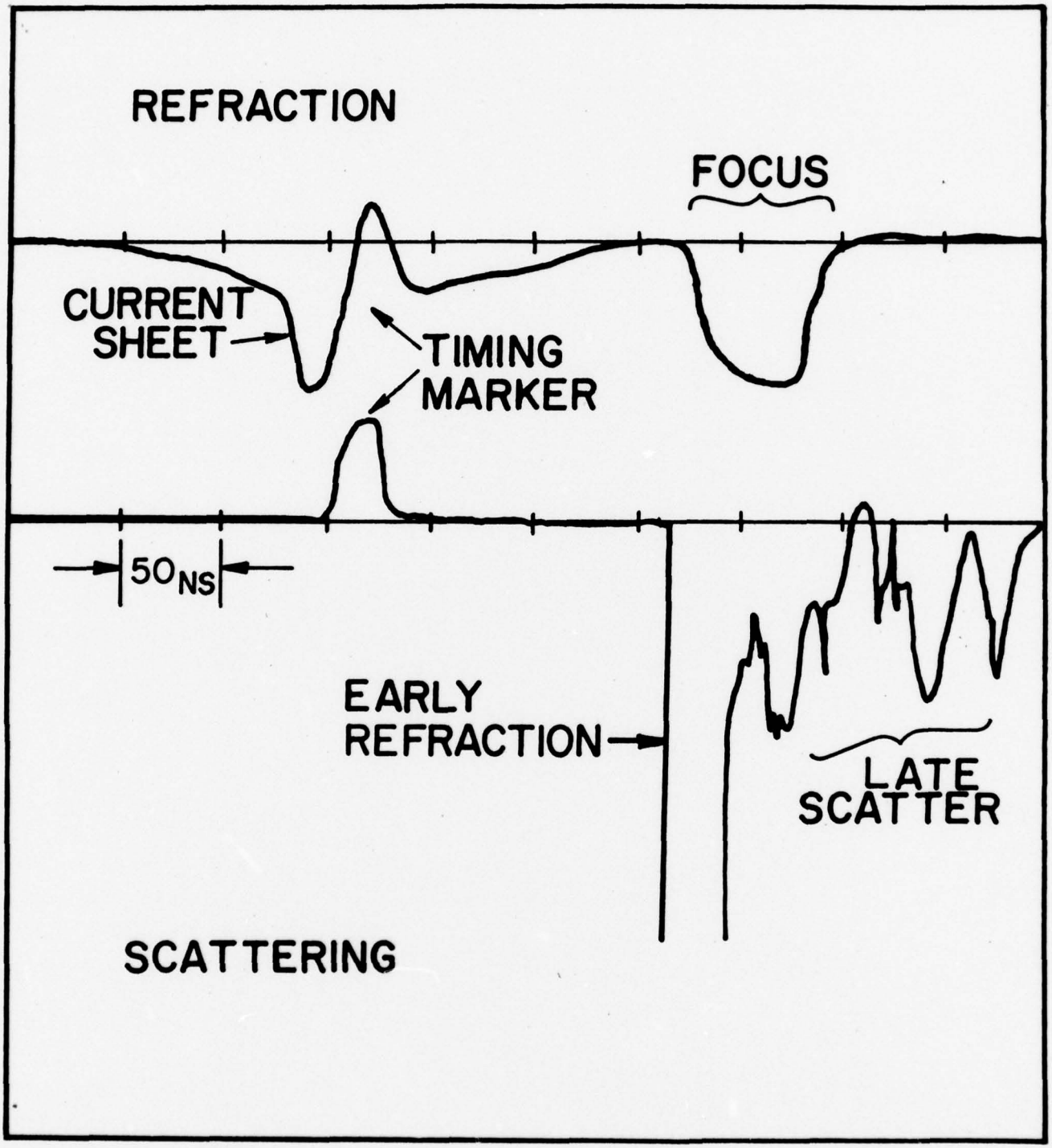
REFRACTION
FOCUS
CURRENT SHEET
TIMING MARKER
50 NS
EARLY REFRACTION
LATE SCATTER
SCATTERING

FIGURE 12

corresponding to a bulk velocity of 1.5×10^5 m/sec, no shift or broadening of the central line was observed.

TIME DEPENDENCE

The time dependence of the signal seemed to rule out bulk refraction from the gross density gradients of the whole pinch since scattering was observed both early in the pinch and later in time. The time dependence of all the diagnostic signals is shown in Figure 13. The data is taken from many shots since we had only two oscilloscopes of sufficient bandwidth (> 100 MHz). Comparative timing was done using timing markers and correcting for time of flight, cable delays, and differences in signal propagation time between oscilloscopes. The resulting accuracy is estimated to be better than $\pm$ 3 ns. There was some shot-to-shot variation between the signals; the most significant occured in the hard X-ray detector with order of magnitude changes in the flux and $\pm$ 15 ns changes in the relative timing. The data in Figure 13 was taken using a fill pressure of .8 torr D_2 with 5% Ar. The peak current was 340 kA. Switching was accomplished with a rather high inductance (> 55 nH) dual trigatron sparkgap. Subsequent data was taken with a low inductance railgap and the scattering volume was closer to the center electrode (5 mm away vs. 12 mm). With the new gap scattering was generally observed early in the pinch in addition to the late scatter observer earlier (See Figure 12).

To determine relative timing of the pinch, a HeNe laser

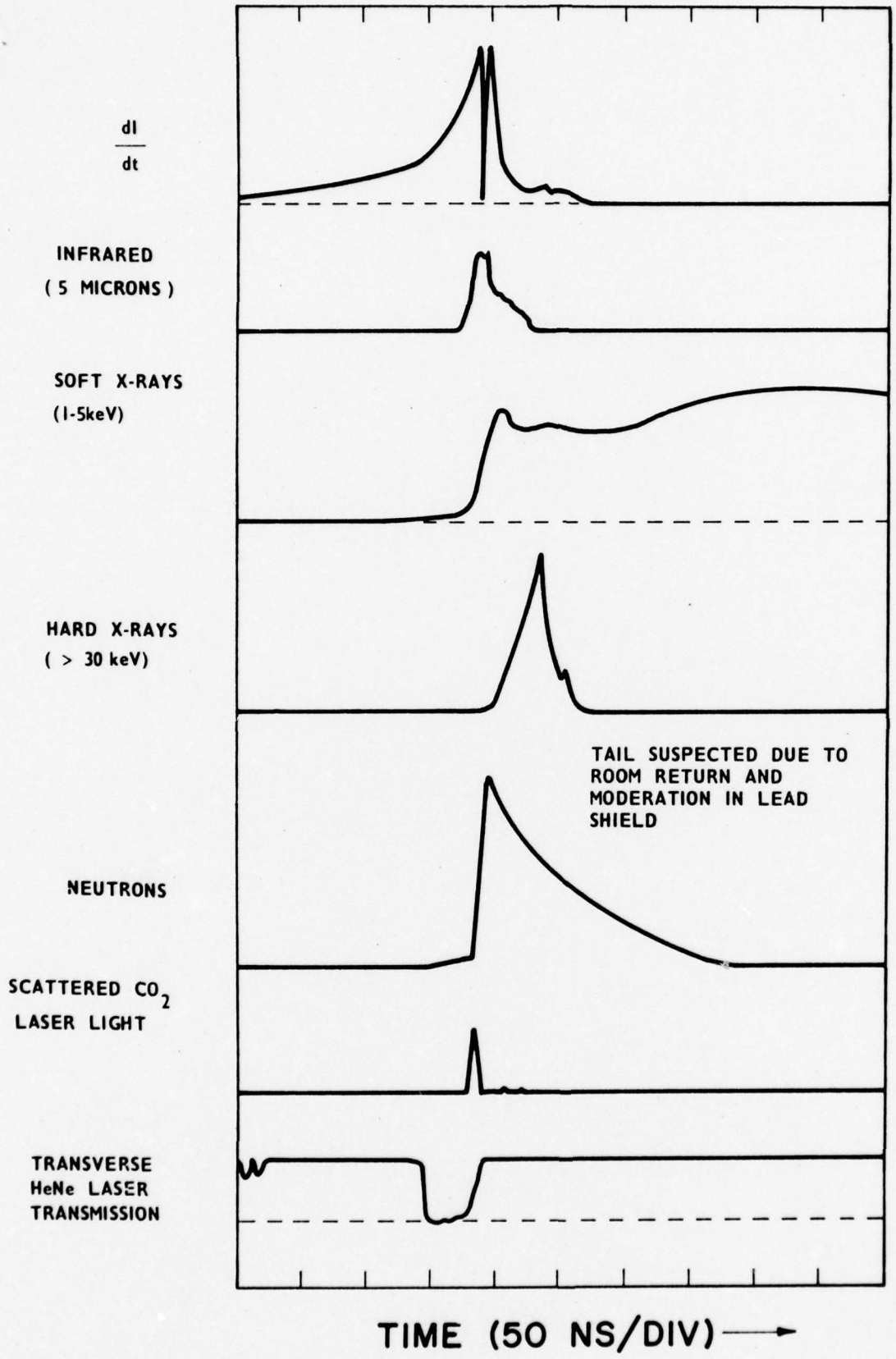
dI/dt
INFRARED
(5 MICRONS)
SOFT X-RAYS
(1-5keV)
HARD X-RAYS
(> 30 keV)
TAIL SUSPECTED DUE TO ROOM RETURN AND MODERATION IN LEAD SHIELD
NEUTRONS
SCATTERED CO_2 LASER LIGHT
TRANSVERSE HeNe LASER TRANSMISSION
TIME (50 NS/DIV) ⟶

FIGURE 13

beam was passed through the scattering volume onto a PIN photodiode. Density gradients typical of the dense pinch ($> 10^{20}$ cm^{-4}) were sufficient to deflect the beam from the diode ($\Delta \phi > 2$ mrad). The early scattering/refraction was stronger and more reproducible at higher currents/filling pressures (450 kA/2.4 torr D_2). At lower pressures/currents (300 kA/.7 torr D_2) where the initial signal was not so overpowering as to obscure the later signal with reflections due to imperfect impedence matching, we observed short duration (usually $\leq$ 5 ns FWHM) spikes of refracted signal late in the pinch and in the post pinch phase.

Neutron production begins early in the pinch but increases by an order of magnitude as the pinch breaks up. Much of the tail on the neutron signal is suspected to be due to room return (scattering into the detector) and to moderation in the lead pig surrounding the scintillator. The wall thickness of the pig is about one mean free path for 2.5 MeV neutrons. Operation of the neutron detector using time of flight separation between the neutrons and X-rays was impractical due to signal blurring due to the energy spread of the neutrons.

Like the neutron signal, the soft X-ray signal also increases greatly as the pinch breaks up. The long tail on that signal is due to line radiation produced by the entrance of copper impurities into the plasma late in time.

The 90^{o} infrared emission peaks with dI/dt which is rather surprising considering the peak in density early in

the pinch. This late peaking is probably due to the gradual increase in Z in the plasma caused by the finite stripping time of the Argon impurity.[8] This effect would have to overcome both the dependence on n^2 (peak density falling) and the weaker $T_e^{-1/2}$ dependence (T_e increasing).

CHAPTER V

SOFT X-RAY PICTURES, DISCUSSION, AND SUMMARY

The observation of high density regions late in time was a surprise since interferograms had not suggested such an occurrence. A size estimate may be made from the maximum scattered power on the detector (.3 W). Assuming total reflection from a hard sphere ($P = \pi r^2 \left(\frac{d\Omega}{4\pi}\right) I \bar{T}$, r is the radius of the sphere, other quantities are as defined in Chapter 4) results in a value of $r = 40\ \mu$. This is the same order as the size of the sources observed on X-ray photos of the focus and explains to a large extent their absence on interferograms. The line density would produce about one fringe which would easily be masked by variations in the return current sheet. Moreover, the scattering indicates these sources last for less than 5 ns so that an overlap in exposure time would be fortuitous.

Although the size of the scattering region was highly suggestive of the micropinches observed on X-ray photographs,[1] the timing of the appearance of these sources was unknown. In order to check the correlation between these bright spots and the scattering, a triple pinhole camera was constructed (See Figure 14). Although Bostick[26] claims the bulk of the radiation exposing the film is in the 1-5 keV range, we observed that the addition of Kimfoil filters had a large

SCHEMATIC OF TRIPLE PINHOLE CAMERA ARRANGEMENT

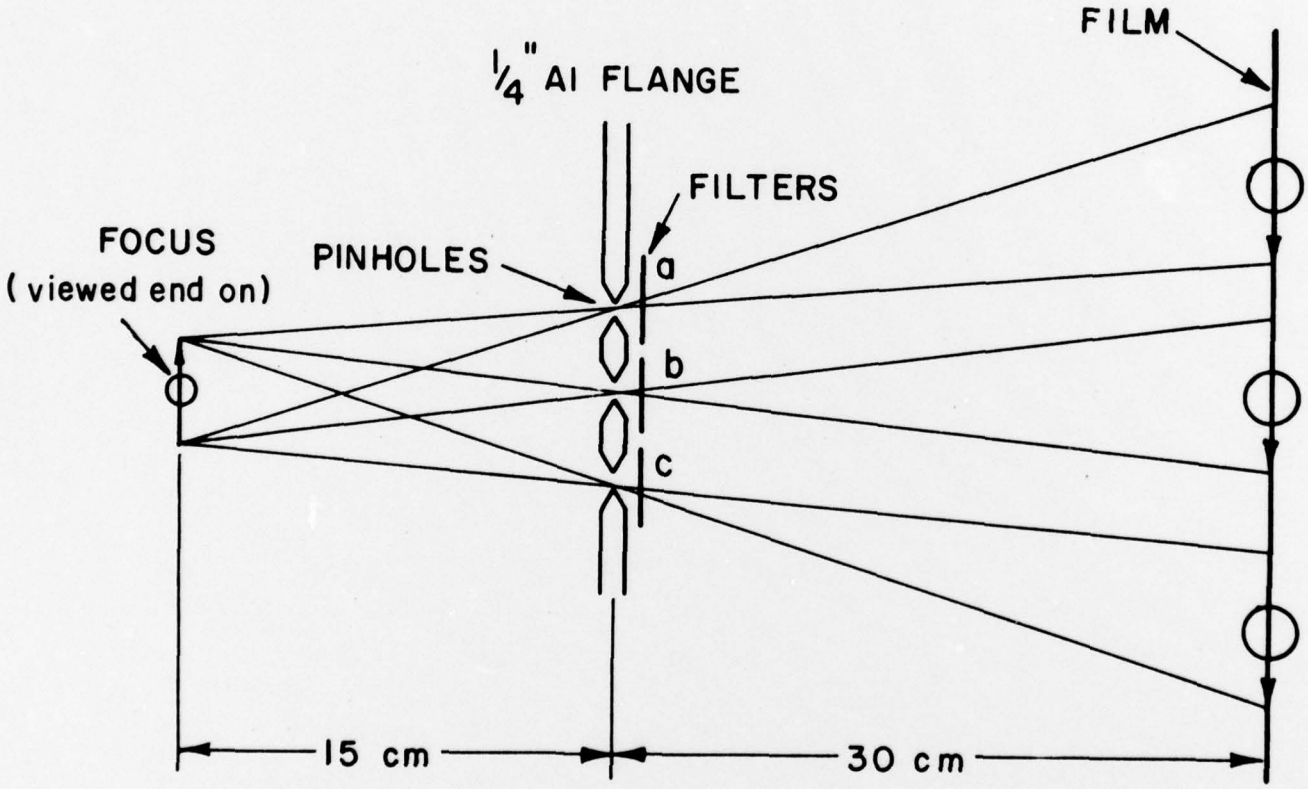

MAGNIFICATION = 2.0

FIGURE 14

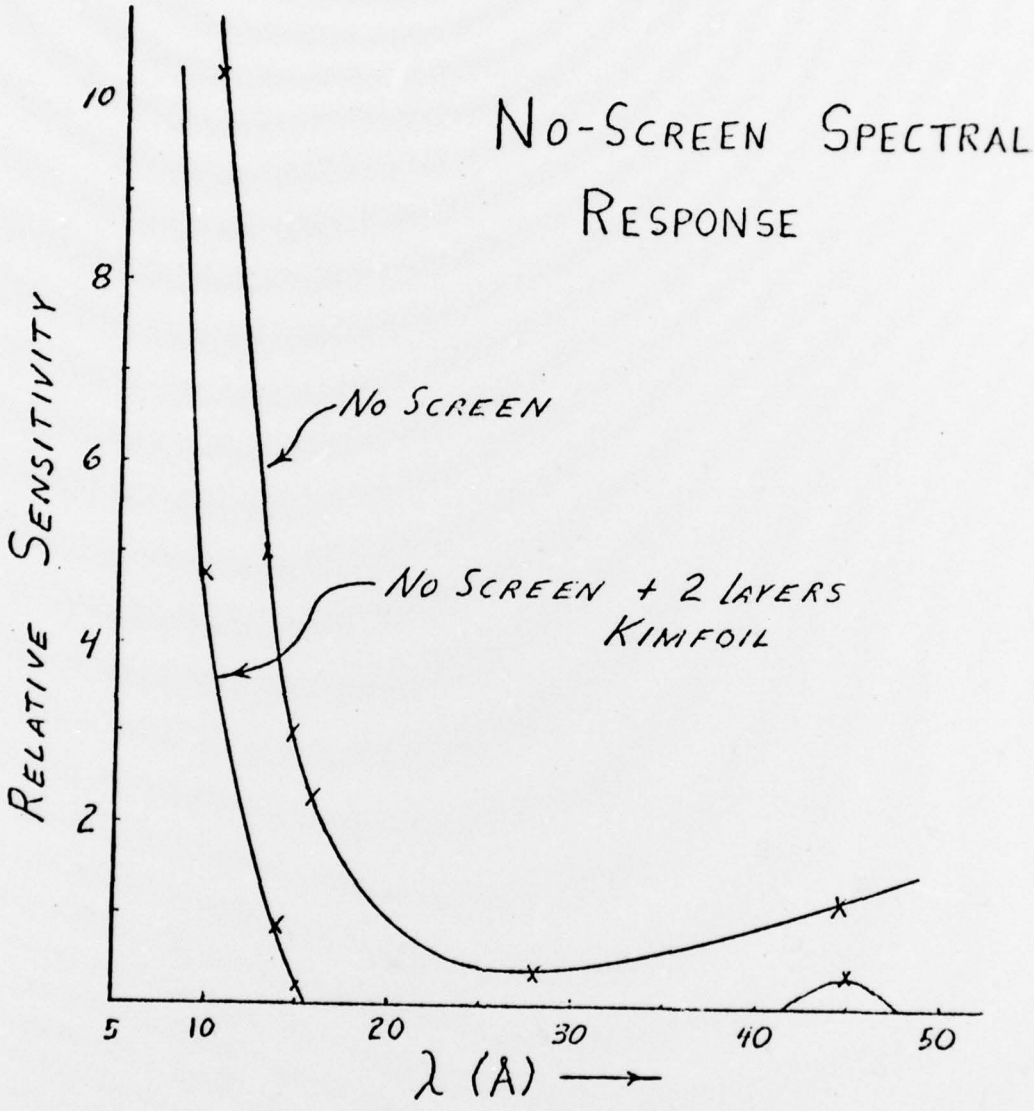

Based on data in Ref. 30 and 31 for a neutral density of .3.

FIGURE 15

effect on the exposure of the negatives. This suggests a lower photon energy (≈.7 - 1. keV) since the transmission of Kimfoil above 1 keV is > 90% (See Figure 15).

Soft X-ray triple pinhole photographs (Figures 16, 17) were taken simultaneously with the scattering experiment. Those cases with bright X-ray spots in the scattering volume always showed scattering late in the pinch or following it, while those which showed no late scattering had no visible spots in the scattering volume although there were sources elsewhere in the pinch volume. A minimum value of $\sim 10^{19}$ cm^{-3} for the density of these micropinches may be inferred from the fact that scattering is occuring from a critical surface for CO_2 laser light. An approximate maximum value for the density may be inferred from the fact that Bernard, et al.[4] also reported seeing short-lived irreproducible signals of $S_k \approx 100$ near the breakup of the pinch with an asymmetric central line profile. The data was taken with a ruby laser at 7^o. Although reflection from a critical surface did presumably not occur, a density of 10^{20} cm^{-3} in a small region would be sufficient to throw considerable power into their detectors. It is worth noting that an experiment performed at 45^o (less subject to refraction) showed scattering levels at a level only three times thermal.[9]

A possible explanation for these short-lived X-ray sources is radiational collapse[17] wherein the radiational loss for a small pinch can exceed its ohmic heating rate leading to an avalanching contraction limited only by the

Soft X-ray Pinhole Photo. Magnification = 2.

Aperature	25μ	100μ	25μ
Filter	Open	2 Kimfoil	Open

----- shows scattering volume

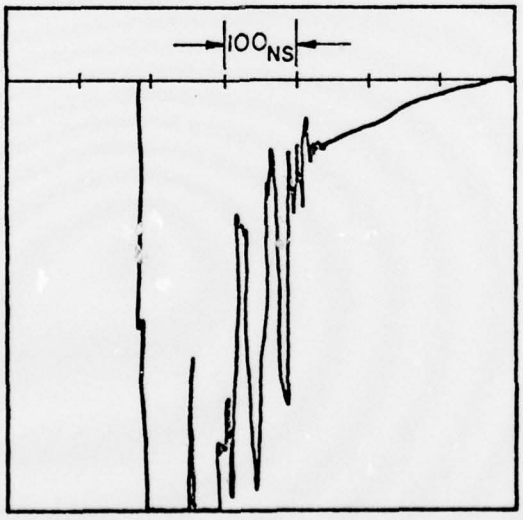

Scattered Signal (.1 V/div)

FIGURE 16

Soft X-ray Pinhole Photo. Magnification = 2.

Aperature	25μ	100μ	25μ
Filter	2 Kimfoil	2 Kimfoil	Open

----- shows scattering volume

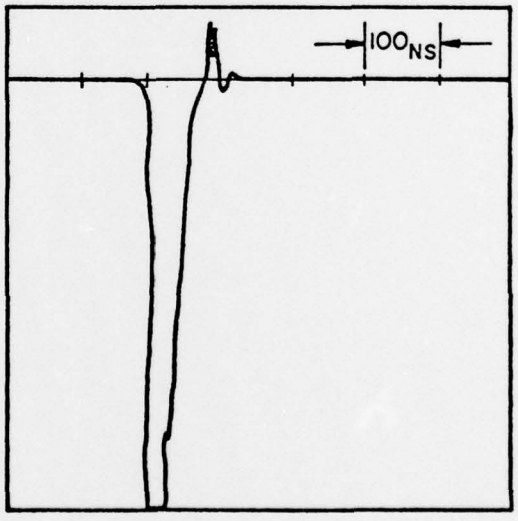

Scattered signal (.1 V/div)

FIGURE 17

growth of some anomalously resistive effect. The correlation between small, dense pinches and X-ray sources has been observed and documented for exploding wire experiments.[25] Despite reports of correlations between the neutron yield and the number and strength of X-ray spots[26], the connection between these micropinches and neutron emission is not clear, as was demonstrated by our last experiment.

In an attempt to frustrate the heating mechanism, a .5 mil tungsten wire was suspended axially in the focus region. Its diameter was small enough so that it would not short out the inductive voltage produced by the collapsing current sheet but would short out any resistively produced voltages in the dense pinch. Proper formation of the focus was still indicated by soft X-ray pictures (Figure 18) including the appearance of the small sources. Neutron production was down by two orders of magnitude in such a case and no spike in dI/dt was observed. Although cooling of the plasma via vaporization of the wire may play a role, one would still expect to see neutron production if the ion acceleration mechanism is directly linked to the source points (turbulence → collective → acceleration). Such is not the case if the mechanism is indirectly linked (turbulence → anomalous resistance → strong $\vec{E}$ field) since this would be shorted out by the wire.

SUMMARY

The experiments performed indicated that the infrared emission from a plasma is a useful diagnostic showing sensi-

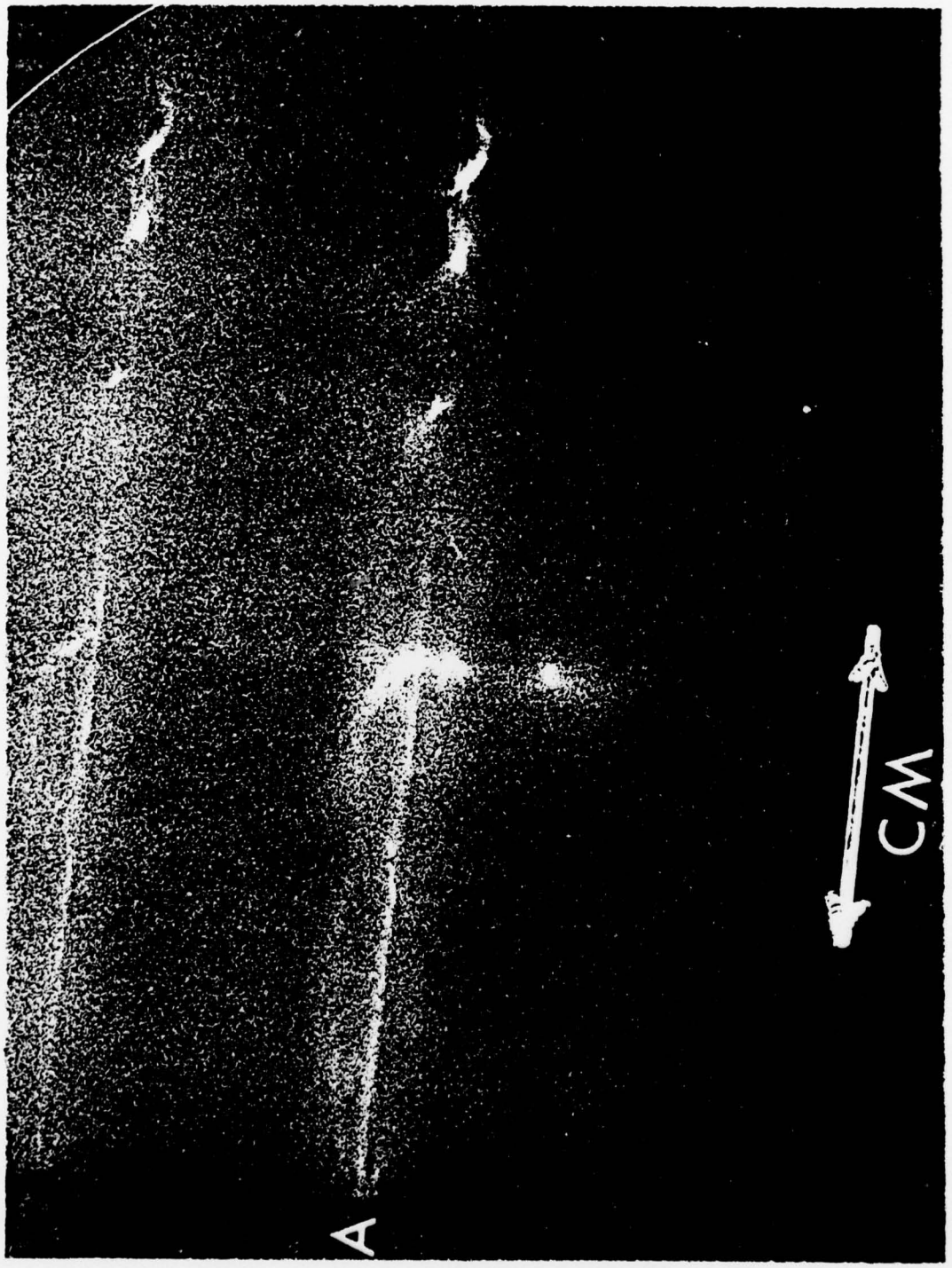

Pinhole Photo of the Focus with $\frac{1}{2}$ mil Tungsten Wire

FIGURE 18

tivity to density in a collisionless plasma and to electron temperature if the plasma is sufficiently collisional to exhibit blackbody dependence. Once calibrated, a cryogenic infrared detector is an easy to use, fast risetime diagnostic. The value of RMS density calculated for our focus was comparable to values obtained on other devices through more elaborate laser interferometric techniques. Absorption by the return current sheet was shown to be significant at 10.6 microns, an important consideration in CO_2 laser heating or scattering experiments.

The collective scattering level of CO_2 light was significant in that it was very low. Reflection from small, dense regions easily dominated any collective scattering signal that might exist. This implies that there is no large volume, high level turbulence. Using soft X-ray pictures, the scattered signal was shown to be correlated with the bright spots of X-ray emission. These spots are therefore characterized by both high density ($\geq 10^{19}$ cm^{-3}) and high electron temperature ($\geq$ 1 keV).

With data from the experiment incorporating a fine wire axially in the focus, the above results suggest indirect action of the micropinches in the heating process. That is to say that although others have shown a correlation between neutron yield and X-ray spots, we have demonstrated that such hot spots are not sufficient for heating to occur. The resolution of these questions will require concurrent use of high resolution, time dependent X-ray photography and high resolution laser interferograms.

APPENDIX

CO_2 LASER

In conjunction with the Plasma Focus Device we built a CO_2 laser of the TEA (Transverse Excited Atmospheric pressure) type. While many designs of such devices have been described in the literature (c.f. Ref. 29), we obtained best results with an adaptation of the design in use at the Naval Research Labs.

A cross section may be seen in Figure 20. The lasing medium is He, CO_2, and N_2 in a 9:1:1 ratio, respectively. The main discharge occurs between the solid aluminum cathode and the transparent anode. Unless a source of free electrons is provided at the cathode, arcs will form preventing lasing. In our case UV produced by an arc along a string of washers provides photoelectrons at the surface of the cathode.

The sparker consists of two parallel rows of small washers 1" apart, center to center. The middle washer in each row is grounded, producing 4 arc chains 14 inches in length. The washers are glued to two layers of .007" mylar which is in turn glued to a copper ground plane. The capacitance between the washers and the ground plane allows the arc to travel down a relatively long string of washers. Although the total arc length is about 2", only 14kV is required for breakdown. The four arc chains, separated by 80 ns isolating

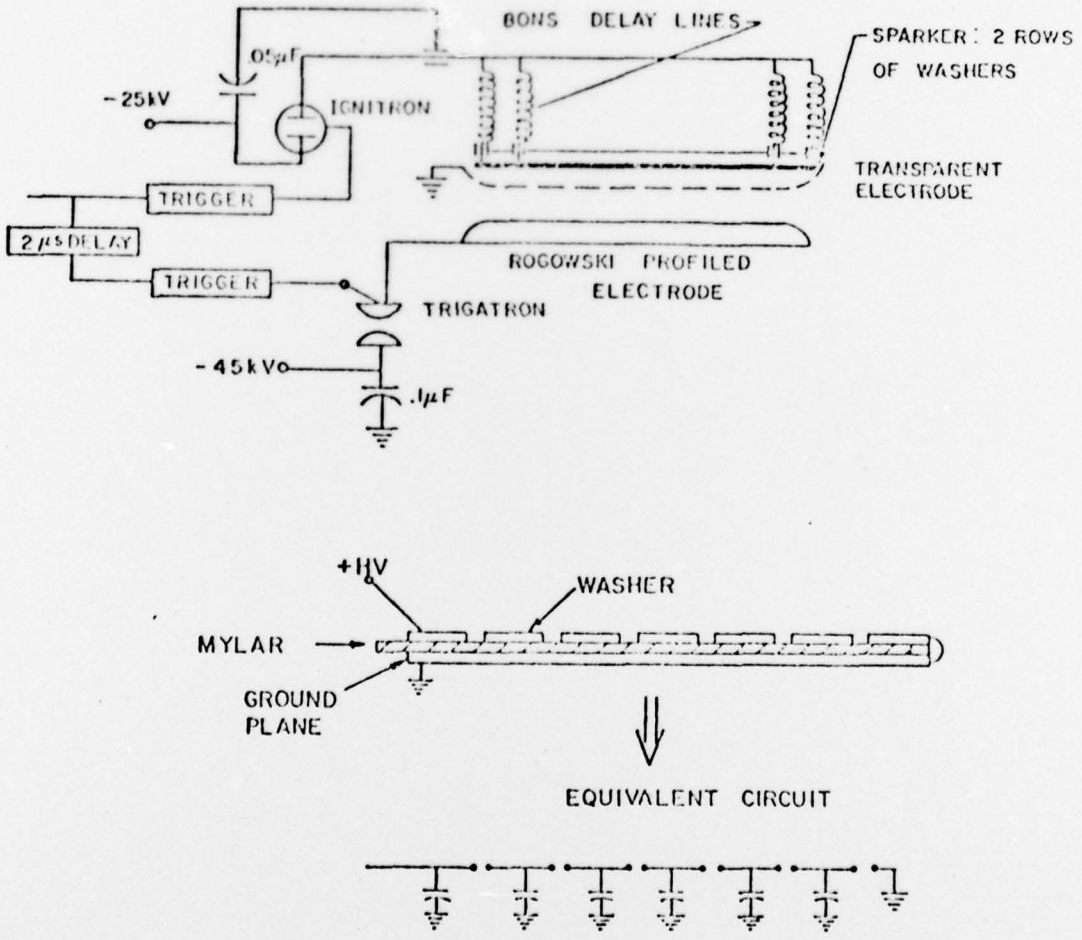
BONS DELAY LINES
SPARKER: 2 ROWS OF WASHERS
.05μF
-25kV
IGNITRON
TRANSPARENT ELECTRODE
TRIGGER
2μs DELAY
TRIGGER
ROGOWSKI PROFILED ELECTRODE
TRIGATRON
-45kV
.1μF
+HV
WASHER
MYLAR
GROUND PLANE
EQUIVALENT CIRCUIT

FIGURE 19

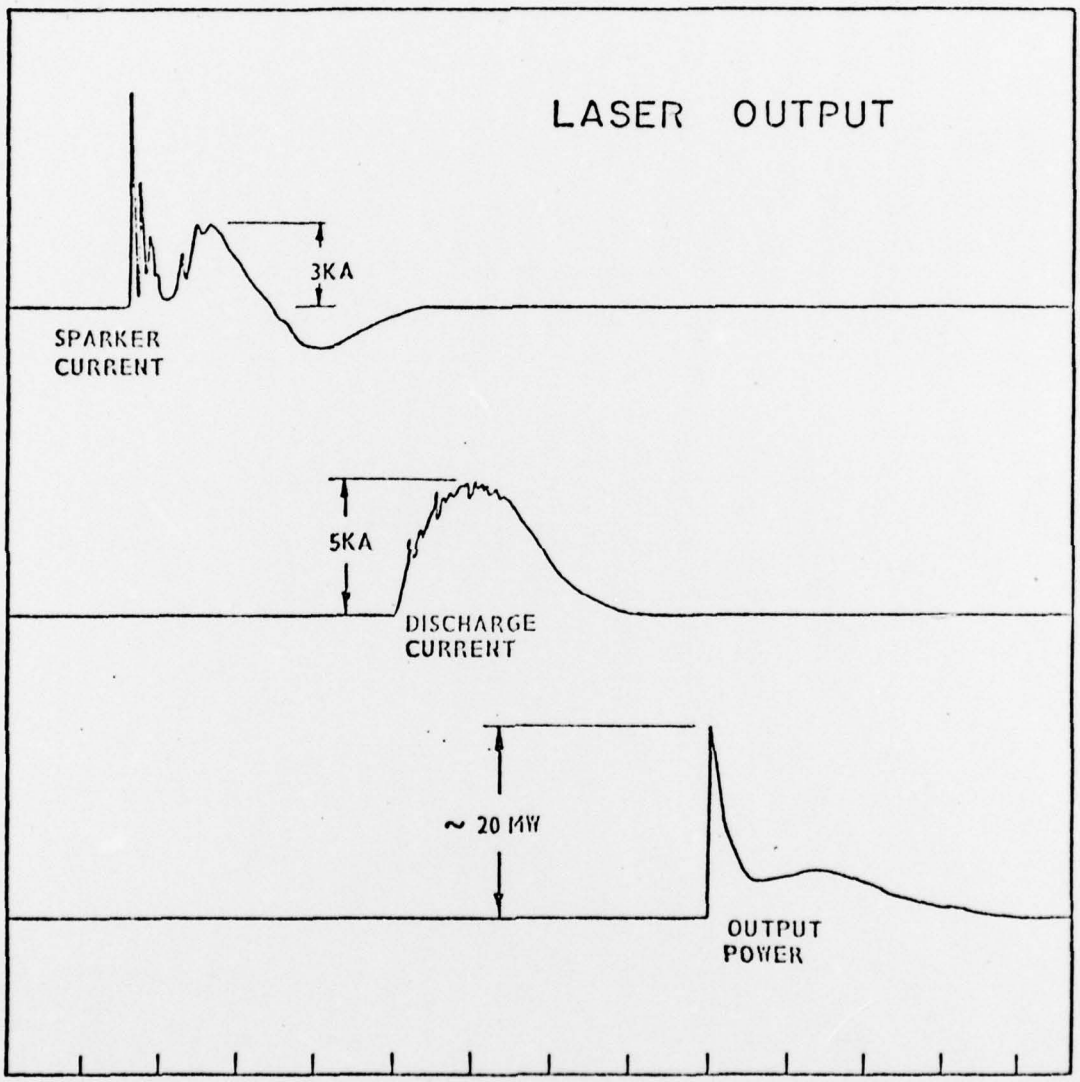
LASER OUTPUT
3KA
SPARKER CURRENT
5KA
DISCHARGE CURRENT
~ 20 MW
OUTPUT POWER
TIME (.5μs / DIV.)

FIGURE 20

delay lines are run from an ignitron switched, .05 microfarad capacitor operated at 25 kV.

The main discharge is driven from a .1 microfarad capacitor. The optimum voltage depends on electrode spacing: 37.5 kV at 1.4". A further increase in voltage at this spacing will cause arcs to form; a decrease will lower output power. The output power is about 20 MW peak with a total energy of about 1.5 joules. A typical output trace is shown in Figure 21. It should be noted that our 1" diameter optics fail to take full advantage of the excited volume.

REFERENCES

1. J. W. Mather in H. A. Griem and R. H. Loveberg, Methods of Experimental Physics, Vol. 9, part A, Academic Press (1970).

2. N. J. Peacock, M. G. Hobby, and P. D. Morgan, Conf. on Plasma Phys. and Controlled Nuclear Fusion Research, Madison, CN-28/D-3 (1971).

3. M. J. Bernstein, D. A. Meskan, and H. L. L. van Paassen, Phys. Fl. 12, 2193 (1969).

4. A. Bernard, A. Coudeville, A. Jolas, J. Launspack, and J. de Mascureau, Phys. Fl. 18, 180 (1975).

5. G. Bekefi, Radiation Processes in Plasmas, John Wiley and Sons, Inc., New York (1966).

6. Santa Barbara Research Center, The Infrared Brochure, No. 716M (1971).

7. R. S. Post, Thesis, Columbia University (1973).

8. N. J. Peacock, R. J. Speer, and M. G. Hobby, Culham Laboratory Report,CLM-P 197 (1969).

9. M. J. Forrest and N. J. Peacock, Culham Laboratory Report CLM-P 349 (1973).

10. David J. Johnson, Rev. Sci. Instrum. 45, 191 (1974).

11. H. L. L. van Paassen, R. H. Vandre, and R. Stephen White, Phys. Fl. 13, 2606 (1970).

12. R. L. Gullickson and H. L. Salin, Bull. A.P.S. II 20, 1236 (1975).

13. P. D. Morgan and N. J. Peacock, Proc. 2nd APS Topical Conf. on Pulsed High Beta Plasmas, Garching (72).

14. V. A. Gribkov, Proc. Conf. on Energy Storage and Compression, Asti-Torino (1974).

15. R. S. Post and T. C. Marshall, Phys. Fl. 17, 452 (1974).

16. Erich S. Weibel, Phys. Rev. Lett. 2, 83 (1959).

17. J. W. Shearer, Phys. Fl. 19, 1426 (1976).

18. Ch. Maisonner, F. Pecorella, J. P. Rager, and M. Samuell, Fifth European Conf. on Cont. Fus. and Pl. Phys. V. II, 183 (1972).

19. R. G. Sagdeev, Fifth European Conf. on Cont. Fus. and Pl. Phys., V. II, 105 (1972).

20. O. Zucker, W. Bostick, R. Gullickson, J. Long, J. Luce, and H. Salin, Proc. Int. Conf. Radiation Test Facilities for the CTR Surface and Materials Program, Argonne (1975).

21. H. Hora and Hannelore Wilhelm, Nuc. Fus. 10, 111 (1970).

22. John Sheffield, Plasma Scattering of Electromagnetic Radiation, Academic Press, New York (1975).

23. M. Kornherr, G. Decker, M. Keilhacker, F. Lindenberger, and H. Rohr, Phys. Lett. 39A 95 (1972).

24. M. Tanimoto, K. Koyama, Y. Matsumoto, and M. Sugira, Conf. on Plasma Phys. and Controlled Nuclear Fusion Research, CN-35/G4-1 (1976).

25. Richard S. Post, David J. Johnson, and Stavros J. Stephanakis, to be published.

26. W. Bostick, V. Nardi, and W. Prior, Annals N.Y. Acad. Sci. 251, 2 (1975).

27. G. R. Neil and R. S. Post, Bull. A. P. S. II 21, 1135 (1976).

28. H. J. Seguin, K. Manes, and J. Tulip, Rev. Sci. Inst. 43, 1134 (1972).

29. J. W. M. Paul, C. C. Daughney, and L. S. Holmes, Nature 223, 822 (1970).

30. David J. Johnson, AFWL-TR-74-43 (1974).

31. Louis N. Koppel, Adv. in X-ray Analysis 18, 146 (1974).